Precambrian Research 354 (2021) 106078

Contents lists available at ScienceDirect

Precambrian Research

journal homepage: www.elsevier.com/locate/precamres

U–Pb–Hf–O–Nd isotopic and geochemical constraints on the origin of Archean TTG gneisses from the North China Craton: Implications for crustal growth

Zhuang Li [a,b,e,f,*], Chunjing Wei [c,*], Bin Chen [d], Wei Zhang [a,b], Fan Yang [a,b]

[a] State Key Laboratory of Petroleum Resources and Prospecting, China University of Petroleum (Beijing), Beijing 102249, China
[b] College of Geosciences, China University of Petroleum (Beijing), Beijing 102249, China
[c] MOE Key Laboratory of Orogenic Belts and Crustal Evolution, School of Earth and Space Sciences, Peking University, Beijing 100871, China
[d] Department of Earth and Space Sciences, Southern University of Science and Technology, Shenzhen 518055, China
[e] Key Laboratory of Regional Geology and Mineralization, Hebei GEO University, Shijiazhuang 050031, China
[f] Key Laboratory of Mineral Resources Evaluation in Northeast Asia, Ministry of Nature and Resources, Changchun 130061, China

ARTICLE INFO

Keywords:
U–Pb–Hf–O–Nd isotope
TTG
Neoarchean
Crustal growth
North China Craton

ABSTRACT

Tonalite–trondhjemite–granodiorite (TTG), an Archean dominant lithological assemblage within the cratonic provinces, is believed to have been formed by partial melting of the hydrous basalts in the garnet stability field. The origin of TTG is a window to decipher the evolution of Archean continental crust, whereas the petrogenesis is not well constrained. To solve this issue, we have carried out field observations, zircon U–Pb–Hf–O isotope, as well as whole-rock Nd–O isotope and geochemical analyses on the TTG and associated dioritic gneisses from the North China Craton. U–Pb isotopic dating using the LA–ICP–MS on zircons reveals that the granitoid gneisses in northern Liaoning were contemporaneously generated during *ca.* 2.56–2.51 Ga and immediately experienced a regional metamorphic event at 2.48–2.45 Ga. The dioritic gneisses occur as quenched inclusions with rounded to ellipsoidal globules in shape rather than lithospheric relics. Such occurrence, together with isotopic and geochemical data, suggests that the mafic enclaves and host TTG represent two co-existing, compositionally distinct magmas. The TTG gneisses are featured by elevated SiO_2 (64.72–86.46 wt%) contents, $(La/Yb)_N$ (68 on average) and Sr/Y (119 on average) ratios, and low MgO (0.35–2.58 wt%) contents and $Mg^{\#}$ values, with radiogenic Hf and Nd isotopes ($\varepsilon_{Hf}(t) = +3.5$ to $+9.0$ and $\varepsilon_{Nd}(t) = +0.8$ to $+5.4$), indicating the derivation from partial melting of the juvenile basaltic sources at lower crustal levels. Compared with the TTG gneisses, the dioritic gneisses have lower SiO_2 contents, higher MgO contents and $Mg^{\#}$ values, with similar Hf–Nd isotopes ($\varepsilon_{Hf}(t) = +3.6$ to $+9.5$ and $\varepsilon_{Nd}(t) = +3.3$ to $+5.1$), implying the depleted mantle source. A model is proposed whereby partial melts from juvenile basaltic sources evolved via mixing with mafic enclaves (viz. dioritic magma) and fractional crystallization, and finally were contaminated by the sedimentary rocks, forming the TTG magma. The granitoid gneisses in northern Liaoning witnessed the major vertical growth of continental crust at the end of the Neoarchean, which is supported by Hf–Nd–O isotopic data and zircon Hf–O isotopic modeling. Our results show that the geochemistry of TTG (such as elevated La/Yb and Sr/Y) might be affected by complex petrogenetic processes, i.e., partial melting of individual sources, magma mixing, fractional crystallization, and crustal contamination, rather than solely controlled by the P–T conditions of crustal anataxis as previously thought, which might have been also overlooked in other Archean cratons.

1. Introduction

Tonalite-trondhjemite-granodiorite (TTG) suite constitutes the major component of the Archean granite–greenstone terranes on Earth, and plays a fundamental role on the formation and evolution of Archean continental crust (Anhaeusser, 2014; Arndt, 2013; Condie, 1981, 1994, 2005; Martin, 1994, 1999; Martin et al., 2005; Smithies et al., 2003; Windley, 1995). It is broadly accepted that the continental crust was mainly generated during three major stages at 3.5–3.2, 2.7 and 2.5 Ga (Condie, 1986, 1998; Condie and Kröner, 2011; Hawkesworth and

* Corresponding authors at: State Key Laboratory of Petroleum Resources and Prospecting, China University of Petroleum (Beijing), Beijing 102249, China.
E-mail addresses: lizhuangcc@pku.edu.cn (Z. Li), cjwei@pku.edu.cn (C. Wei).

https://doi.org/10.1016/j.precamres.2020.106078
Received 18 June 2020; Received in revised form 31 August 2020; Accepted 19 December 2020
Available online 6 January 2021

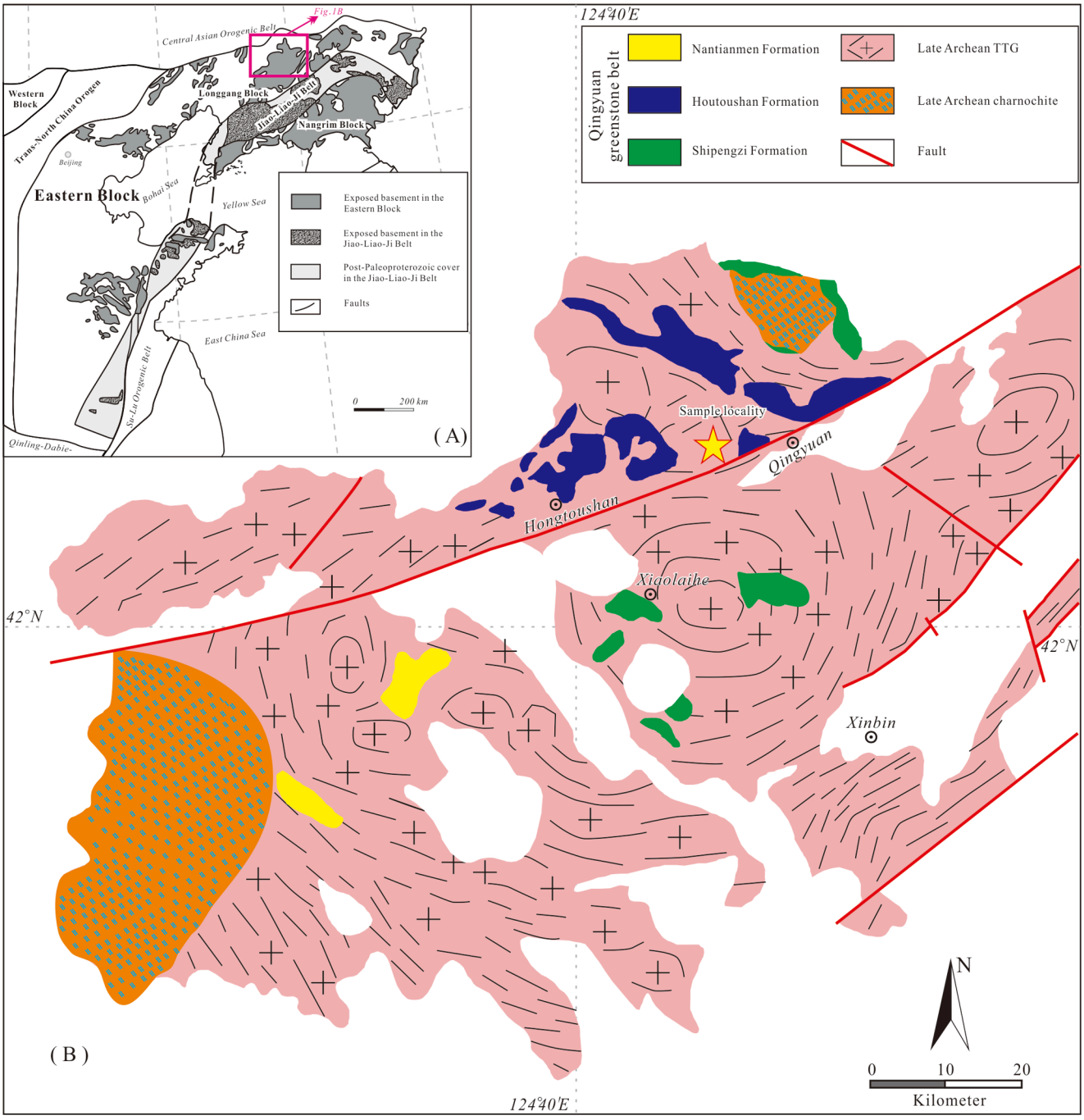

Fig. 1. (A) The distribution of the Archean to Paleoproterozoic basement in the North China Craton (after Zhao et al., 2001, 2005, 2012; Zhao and Zhai, 2013). (B) Geological sketch map of the Qingyuan granite–greenstone terrane (after Li and Shen, 2000; Li and Wei, 2017; Wan et al., 2005a; Peng et al., 2015; Zhai et al., 1985).

Kemp, 2006; Hill et al, 1992). Among these crustal formation periods, the early Neoarchean is significant for the formation of the granite–-greenstone worldwide (Hollings et al, 1999; Lodge, 2016; Xie et al., 1993), whereas TTGs with late Neoarchean age have been regionally identified in a few cratons, such as the Antarctic Craton, South India Craton, West African Craton and North China Craton, and thus attracted less attraction (Clark et al., 2009, 2012; Geng et al., 2006a, 2012b, 2012c; Maibam et al., 2016; Wu et al., 2013, Wu et al., 2016; Yang et al., 2008; Zhao and Zhai, 2013; Zhao et al., 1998, 2001; Condie, 2005). The North China Craton, one of the few cratons, voluminously expose TTGs with ages spreading from Eoarchean to Neoarchean, yielding a peak at *ca.* 2.5 Ga (Geng et al., 2006, 2012; Zhai and Santosh, 2013; Zhao and Zhai, 2013; Zhao et al., 2005, 2012), which provides a possibility to decoding crustal growth in the early Precambrian and making the early stages of Earth's evolution to be better understood. Although extensive studies on geochemistry and geochronology of volcanic rocks within the greenstone belts (Bai et al., 2014; Li and Shen, 2000; Li and Wei, 2017; Wan et al., 2005a, 2005b; Wu et al., 2016) and granitoid gneisses (Grant et al., 2009; Wang et al., 2016a, 2016b; Li et al., 2019b, Li et al., 2019c, Li et al., 2020; Yang et al., 2008), metamorphism of the greenstone belts (Wu et al., 2013; Yang and Wei, 2017a, 2017b), field structures (Shen et al., 1997; Zhai et al., 1985), and/or a combination of these approaches (Peng et al., 2015; Zhai and Santosh, 2013; Zhao and Zhai, 2013; Zhao et al., 2005, 2012) have been conducted, controversies regarding the nature for the late Neoarchean crustal evolution of the North China Craton still remain (Zhao and Zhai, 2013). Some researchers favored

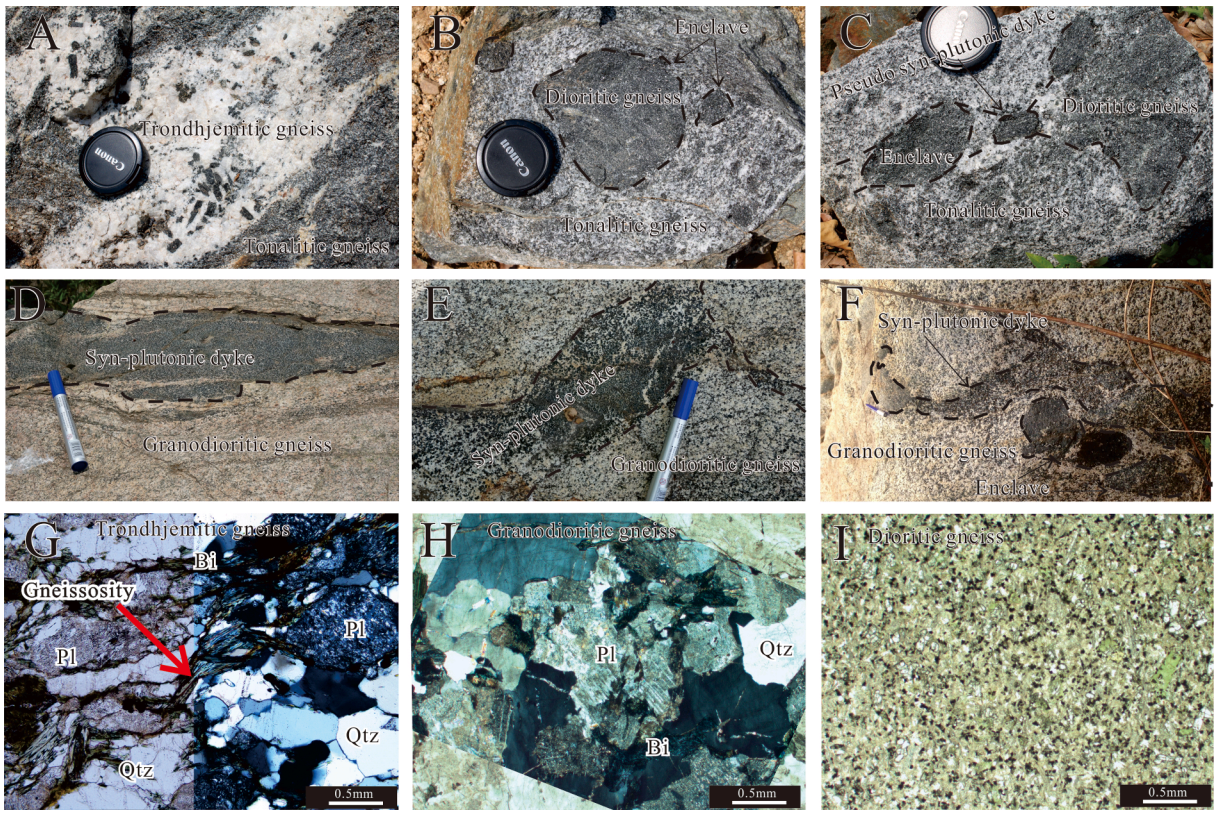

Fig. 2. (A–F) Photographs of an outcrop and (G–I) photomicrographs of the granitoid gneisses. Pl, plagioclase; Bi, biotite; Qtz, quartz.

major crustal growth during late Neoarchean (Grant et al., 2009; Li et al., 2020; Liu et al., 2008; Polat et al., 2005; Wu et al., 2016). In contrast, others argued that the late Neoarchean tectono-thermal event is just a reworking event overprinting the pre-existing continental crustal materials, and suggested that the major juvenile crust mainly grew during early Neoarchean (Bai et al., 2014; Geng et al., 2006, 2012; Jiang et al., 2010; Liu et al., 2017). Such a controversy arises from lacking of a systematic petrogenesis study on the late Neoarchean rocks in the North China Craton (Zhai and Santosh, 2013; Zhao and Zhai, 2013). Hence, the TTG gneisses from the North China Craton (e.g., northern Liaoning) would be one of the best candidates to decipher the nature of the late Neoarchean tectono-thermal event due to volumetrically 70–80% of the exposed Precambrian crystalline basement (Li and Chen, 2019).

A wealth of studies reveal that the TTG mainly originated from the partial melting of hydrous basalts in the garnet stability field, e.g., garnet amphibolite and eclogite (Atherton and Petford, 1993; Martin, 1986; Moyen, 2011; Moyen and Stevens, 2006), resulting in the salient geochemical features analogy to the Cenozoic adakite ($SiO_2 \geq 56$ wt%, high Sr/Y (≥40) and La /Yb (≥20), and strongly depleted in Y (≤18 ppm) and Yb (≤1.9 ppm); Martin, 1994, 1999; Martin et al., 2005). Thus geochemistry (e.g., elevated Sr/Y or La/Yb ratios) of the TTG was used to deduce the depth of melting (Castillo, 2012; Moyen, 2009). Conspicuously, TTG is an essentially part of granitoid, whose geochemistry would not only be controlled by *P–T* conditions during the partial melting, but also the source compositions and magmatic processes (Arth and Barker, 1976; Castillo et al., 1999; Wu et al., 2007). In other words, the nature of the magma sources (enriched versus depleted basalts), magma mixing, fractional crystallization, and crustal contamination can also contribute to the geochemical characteristics, which have been overlooked in the petrogenetic investigations of the TTG (Condie, 1981, 1986, 1994, 1998; Li and Wei, 2017). In addition, there is still a "missing link" between the TTG and mafic enclave, which might be essential to decipher the nature of the TTG, and few data for this are available (Li et al., 2019b, 2019c).

In this contribution, we propose further constraints on these issues by studying the Neoarchean TTG gneisses in northern Liaoning, eastern North China Craton. Particularly, a combination of field investigation, U–Pb–Hf–O–Nd isotopic and geochemical data were used to investigate the age and source characteristics of the Neoarchean TTG gneisses in northern Liaoning, and illustrate the detailed magmatic processes and crustal growth of the North China Craton as well.

2. Geological background

The North China Craton, the largest craton in China with 300 000 km^2 in area, is bounded by the Paleozoic Central Asian Orogenic Belt to the north and by the Kunlun-Qinling–Dabie–Su–Lu Orogenic Belt to the south (Fig. 1A; Zhao and Zhai, 2013). It is one of the oldest continental nuclei on Earth, containing 3.85 Ga trondhjemite (Li and Chen, 2019; Liu et al., 2008; Song et al., 1996; Wan et al., 2005c, 2012) and zircons with an age of >4.0 Ga (Li et al., 2016b). An issue of major dispute in the North China Craton is the subdivisions of the Neoarchean–Paleoproterozoic basement, including at least two prevalent models (Zhao and Zhai, 2013). Zhai and Santosh (2013) envisaged that cratonization of the North China Craton occurred at *ca.* 2.5 Ga through amalgamation of micro-blocks and island arcs, followed by a Paleoproterozoic imprint. The other more popular model attested that it was formed through the assembly of the Eastern and Western blocks along the Trans-North China Orogen (Polat et al., 2005; Zhao and Zhai, 2013; Zhao et al., 2005). The Eastern Block comprises the Archean Longgang Block in the north, the Archean Nangrim Block in the south, and the intervening Paleoproterozoic Jiaoliao Mobile Belt or Jiao–Liao–Ji Belt (Li et al., 2016a, 2017, 2019a; Zhao and Zhai, 2013; Zhao et al., 2005).

The Qingyuan granite–greenstone terrane within the northern Longgang Block is dominated by granitoid gneisses, and minor supracrustal sequences (Fig. 1B; Shen et al., 1997), which is divided by the NE–trending Hunhe shear zone into two parts (Wan et al., 2005a, b).

Table 1
Zircon U–Pb data.

Spot	Th	U	Th/U	Isotopic ratios					Corrected ages (Ma)							Disc (%)
	(ppm)	(ppm)		$^{207}Pb/^{206}Pb$	1σ	$^{207}Pb/^{235}U$	1σ	$^{206}Pb/^{238}U$	1σ	$^{207}Pb/^{206}Pb$	1σ	$^{207}Pb/^{235}U$	1σ	$^{206}Pb/^{238}U$	1σ	
15LQ07-1	Dioritic gneiss															
	Magmatic zircon															
15LQ07-1-01	60	135	0.45	0.1748	0.0043	12.05	0.31	0.4975	0.0057	2606	46	2608	24	2603	25	0.09
15LQ07-1-02	62	152	0.41	0.1766	0.0037	11.69	0.24	0.4770	0.0042	2621	35	2580	20	2514	18	4.08
15LQ07-1-03	29	57	0.51	0.1732	0.0043	11.23	0.28	0.4683	0.0048	2589	41	2542	23	2476	21	4.34
15LQ07-1-04	46	49	0.94	0.1723	0.0044	11.34	0.30	0.4746	0.0060	2580	42	2552	25	2504	26	2.96
15LQ07-1-06	44	111	0.39	0.1643	0.0038	11.42	0.27	0.5007	0.0054	2502	39	2558	22	2617	23	−4.59
15LQ07-1-07	19	27	0.69	0.1628	0.0050	11.03	0.33	0.4915	0.0072	2487	52	2526	28	2577	31	−3.63
15LQ07-1-08	30	65	0.46	0.1716	0.0043	11.28	0.27	0.4745	0.0053	2573	43	2546	22	2503	23	2.71
15LQ07-1-09	40	70	0.58	0.1665	0.0037	11.35	0.25	0.4905	0.0049	2524	38	2553	21	2573	21	−1.93
15LQ07-1-10	14	38	0.38	0.1645	0.0043	11.22	0.30	0.4919	0.0070	2503	44	2541	25	2579	30	−3.05
15LQ07-1-12	21	30	0.72	0.1581	0.0052	10.01	0.31	0.4574	0.0063	2435	60	2435	29	2428	28	0.30
15LQ07-1-13	68	74	0.91	0.1640	0.0040	11.07	0.27	0.4837	0.0054	2498	41	2529	23	2544	24	−1.82
15LQ07-1-14	99	249	0.40	0.1587	0.0032	10.16	0.20	0.4591	0.0038	2443	34	2449	18	2436	17	0.28
15LQ07-1-16	23	31	0.73	0.1587	0.0039	11.12	0.27	0.5060	0.0061	2442	42	2533	23	2639	26	−8.10
15LQ07-1-17	42	70	0.60	0.1623	0.0037	10.79	0.25	0.4802	0.0052	2479	39	2506	22	2528	23	−1.97
15LQ07-1-19	40	98	0.41	0.1615	0.0040	11.14	0.28	0.4976	0.0053	2471	42	2534	24	2604	23	−5.35
15LQ07-1-20	80	127	0.63	0.1599	0.0034	10.87	0.24	0.4912	0.0054	2454	36	2512	20	2576	24	−4.97
15LQ07-1-21	28	35	0.79	0.1681	0.0047	11.25	0.31	0.4863	0.0073	2539	47	2544	26	2555	32	−0.64
15LQ07-1-24	68	171	0.40	0.1636	0.0039	11.17	0.27	0.4897	0.0059	2494	39	2537	23	2569	25	−3.01
15LQ07-1-26	46	63	0.73	0.1696	0.0040	11.53	0.27	0.4889	0.0049	2554	40	2567	22	2566	21	−0.47
15LQ07-1-27	79	72	1.10	0.1699	0.0037	11.58	0.26	0.4905	0.0051	2557	37	2571	21	2573	22	−0.61
15LQ07-1-28	25	36	0.69	0.1679	0.0047	11.79	0.34	0.5062	0.0060	2539	42	2588	27	2640	26	−3.99
15LQ07-1-30	28	34	0.82	0.1717	0.0051	11.30	0.34	0.4781	0.0058	2576	50	2548	28	2519	25	2.21
15LQ07-1-31	40	47	0.85	0.1696	0.0050	10.97	0.32	0.4701	0.0054	2554	50	2521	27	2484	24	2.74
15LQ07-1-34	43	47	0.92	0.1637	0.0040	10.90	0.26	0.4799	0.0052	2494	73	2514	23	2527	23	−1.30
15LQ07-1-35	32	42	0.75	0.1702	0.0045	11.66	0.29	0.4945	0.0051	2559	44	2577	24	2590	22	−1.22
15LQ07-1-36	30	40	0.75	0.1730	0.0046	12.09	0.32	0.5038	0.0071	2587	45	2612	25	2630	31	−1.65
15LQ07-1-37	29	46	0.63	0.1738	0.0046	12.55	0.32	0.5192	0.0062	2595	44	2647	24	2696	27	−3.89
15LQ07-1-38	52	50	1.05	0.1723	0.0042	11.99	0.29	0.5007	0.0052	2581	41	2603	22	2617	22	−1.40
15LQ07-1-39	27	30	0.91	0.1622	0.0046	11.04	0.30	0.4922	0.0052	2479	48	2526	25	2580	23	−4.07
15LQ07-1-40	105	189	0.56	0.1686	0.0032	11.96	0.23	0.5100	0.0045	2544	32	2601	18	2657	19	−4.42
15LQ07-1-42	60	53	1.12	0.1645	0.0043	11.07	0.29	0.4878	0.0059	2502	44	2529	24	2561	26	−2.35
15LQ07-1-43	172	275	0.63	0.1653	0.0035	9.95	0.23	0.4341	0.0043	2511	35	2430	21	2324	19	7.43
15LQ07-1-44	46	46	0.98	0.1729	0.0042	11.75	0.28	0.4919	0.0059	2587	40	2585	23	2579	26	0.32
15LQ07-1-47	35	40	0.86	0.1604	0.0042	10.53	0.27	0.4735	0.0055	2461	44	2483	24	2499	24	−1.53
15LQ07-1-48	36	50	0.72	0.1614	0.0042	10.70	0.28	0.4767	0.0057	2472	43	2497	24	2513	25	−1.65
15LQ07-1-51	36	63	0.57	0.1593	0.0039	9.96	0.23	0.4521	0.0049	2450	47	2431	21	2405	22	1.85
15LQ07-1-53	66	54	1.23	0.1577	0.0038	10.85	0.26	0.4976	0.0057	2431	40	2510	23	2603	25	−7.08
15LQ07-1-54	30	140	0.21	0.1678	0.0048	11.09	0.32	0.4797	0.0065	2535	48	2531	27	2526	28	0.37
15LQ07-1-55	48	57	0.84	0.1635	0.0042	13.13	0.38	0.5829	0.0114	2492	42	2689	28	2960	47	−18.78
15LQ07-1-56	498	589	0.85	0.1617	0.0031	10.78	0.22	0.4811	0.0051	2473	32	2505	19	2532	22	−2.39
15LQ07-1-58	50	118	0.42	0.1637	0.0034	11.34	0.25	0.4990	0.0056	2495	35	2552	21	2610	24	−4.60
15LQ07-1-59	43	66	0.66	0.1669	0.0041	13.10	0.31	0.5671	0.0062	2527	40	2687	23	2896	26	−14.60
15LQ07-1-60	182	359	0.51	0.1670	0.0037	11.36	0.25	0.4891	0.0046	2528	37	2553	21	2567	20	−1.54
	Metamorphic zircon															
15LQ07-1-05	59	242	0.24	0.1633	0.0033	10.75	0.22	0.4741	0.0045	2490	33	2502	19	2502	20	−0.44
15LQ07-1-11	47	293	0.16	0.1617	0.0033	10.52	0.20	0.4668	0.0043	2473	34	2482	18	2469	19	0.15
15LQ07-1-15	17	105	0.17	0.1599	0.0033	10.39	0.21	0.4678	0.0047	2455	40	2470	19	2474	21	−0.78
15LQ07-1-22	41	128	0.32	0.1559	0.0032	10.31	0.21	0.4760	0.0041	2413	35	2463	18	2510	18	−4.02
15LQ07-1-23	53	149	0.35	0.1573	0.0033	10.61	0.22	0.4842	0.0049	2427	36	2489	20	2545	21	−4.86
15LQ07-1-25	7	45	0.16	0.1611	0.0046	10.66	0.30	0.4767	0.0061	2478	47	2494	26	2513	27	−1.41

(*continued on next page*)

Table 1 (*continued*)

Spot	Th	U	Th/U	Isotopic ratios						Corrected ages (Ma)							Disc (%)
	(ppm)	(ppm)		$^{207}Pb/^{206}Pb$	1σ	$^{207}Pb/^{235}U$	1σ	$^{206}Pb/^{238}U$	1σ	$^{207}Pb/^{206}Pb$	1σ	$^{207}Pb/^{235}U$	1σ	$^{206}Pb/^{238}U$	1σ		
15LQ07-1-29	7	23	0.29	0.1622	0.0050	10.75	0.33	0.4803	0.0063	2479	52	2502	29	2529	27		−1.99
15LQ07-1-32	52	140	0.37	0.1597	0.0034	10.48	0.23	0.4736	0.0045	2454	36	2478	20	2499	20		−1.85
15LQ07-1-33	37	111	0.34	0.1600	0.0036	11.10	0.25	0.5017	0.0061	2457	38	2531	21	2621	26		−6.66
15LQ07-1-41	31	171	0.18	0.1643	0.0033	10.14	0.21	0.4446	0.0039	2502	34	2448	19	2371	17		5.22
15LQ07-1-45	40	205	0.19	0.1587	0.0032	10.52	0.21	0.4779	0.0044	2442	33	2481	19	2518	19		−3.10
15LQ07-1-46	22	145	0.15	0.1578	0.0031	10.28	0.21	0.4694	0.0048	2432	34	2460	19	2481	21		−2.00
	Later-thermal-event zircon																
15LQ07-1-18	30	51	0.59	0.1536	0.0044	10.29	0.29	0.4851	0.0058	2387	50	2461	26	2549	25		−6.80
15LQ07-1-49	56	137	0.41	0.1531	0.0035	9.77	0.22	0.4588	0.0052	2381	39	2414	21	2434	23		−2.23
15LQ07-1-50	53	255	0.21	0.1545	0.0031	9.98	0.20	0.4642	0.0041	2396	35	2433	18	2458	18		−2.58
15LQ07-1-52	6	30	0.20	0.1536	0.0044	9.80	0.27	0.4648	0.0068	2386	49	2417	25	2461	30		−3.13
15LQ07-1-57	3	20	0.17	0.1544	0.0052	9.99	0.35	0.4676	0.0070	2395	56	2434	33	2473	31		−3.24
15LQ08-1	Tonalitic gneiss																
	Magmatic zircon																
15LQ08-1-01	27	120	0.22	0.1671	0.0021	11.24	0.13	0.4881	0.0045	2529	21	2544	11	2562	19		−1.33
15LQ08-1-02	47	72	0.65	0.1716	0.0023	11.65	0.14	0.4924	0.0047	2574	22	2577	11	2581	20		−0.29
15LQ08-1-03	39	73	0.54	0.1717	0.0023	11.52	0.14	0.4868	0.0047	2574	22	2566	11	2557	20		0.67
15LQ08-1-04	35	60	0.58	0.1733	0.0023	11.64	0.15	0.4871	0.0047	2590	22	2576	12	2558	21		1.23
15LQ08-1-05	38	304	0.12	0.1693	0.0021	11.18	0.12	0.4790	0.0042	2551	21	2538	10	2523	18		1.09
15LQ08-1-06	36	93	0.39	0.1682	0.0022	10.62	0.13	0.4581	0.0043	2540	22	2490	11	2431	19		4.27
15LQ08-1-10	49	74	0.66	0.1726	0.0023	11.60	0.14	0.4876	0.0046	2583	22	2573	11	2560	20		0.86
15LQ08-1-12	20	94	0.21	0.1708	0.0024	11.53	0.15	0.4898	0.0048	2566	23	2567	12	2570	21		−0.17
15LQ08-1-13	162	176	0.92	0.1706	0.0022	11.23	0.13	0.4775	0.0043	2563	21	2542	11	2516	19		1.83
15LQ08-1-14	52	67	0.77	0.1714	0.0023	11.35	0.14	0.4806	0.0046	2571	23	2552	12	2530	20		1.60
15LQ08-1-15	48	75	0.64	0.1720	0.0023	11.52	0.14	0.4861	0.0046	2577	22	2566	12	2554	20		0.89
15LQ08-1-16	49	212	0.23	0.1683	0.0022	11.33	0.13	0.4885	0.0044	2541	21	2551	11	2564	19		−0.92
15LQ08-1-17	25	59	0.42	0.1687	0.0023	11.23	0.14	0.4829	0.0047	2545	23	2542	12	2540	20		0.20
15LQ08-1-18	36	70	0.52	0.1706	0.0024	11.30	0.14	0.4805	0.0046	2564	23	2549	12	2530	20		1.34
15LQ08-1-19	32	87	0.37	0.1660	0.0023	10.98	0.14	0.4798	0.0045	2518	23	2521	12	2526	20		−0.35
15LQ08-1-20	91	132	0.69	0.1695	0.0023	11.18	0.14	0.4783	0.0044	2553	22	2538	11	2520	19		1.30
15LQ08-1-21	94	258	0.36	0.1707	0.0022	11.20	0.13	0.4759	0.0042	2564	22	2540	11	2510	19		2.14
15LQ08-1-23	37	63	0.59	0.1722	0.0024	11.55	0.15	0.4867	0.0048	2579	23	2569	12	2556	21		0.88
15LQ08-1-24	36	79	0.45	0.1688	0.0023	12.15	0.15	0.5223	0.0050	2545	23	2616	12	2709	21		−6.42
15LQ08-1-25	88	130	0.68	0.1701	0.0023	11.59	0.14	0.4943	0.0046	2558	22	2572	11	2589	20		−1.20
15LQ08-1-26	42	70	0.61	0.1709	0.0024	11.23	0.15	0.4766	0.0046	2566	23	2542	12	2512	20		2.10
15LQ08-1-27	84	123	0.68	0.1701	0.0024	11.42	0.15	0.4871	0.0047	2559	23	2558	12	2558	20		0.04
15LQ08-1-28	61	113	0.54	0.1713	0.0026	11.62	0.16	0.4920	0.0051	2570	25	2574	13	2579	22		−0.35
15LQ08-1-29	42	67	0.63	0.1700	0.0025	11.60	0.16	0.4949	0.0051	2557	25	2572	13	2592	22		−1.36
15LQ08-1-30	83	141	0.59	0.1682	0.0023	11.31	0.14	0.4878	0.0045	2540	23	2549	12	2561	19		−0.85
15LQ08-1-31	51	87	0.58	0.1701	0.0024	11.14	0.14	0.4751	0.0045	2559	23	2535	12	2506	20		2.07
15LQ08-1-34	16	43	0.36	0.1738	0.0028	11.86	0.18	0.4950	0.0056	2594	27	2593	15	2592	24		0.08
15LQ08-1-35	28	54	0.53	0.1698	0.0025	11.47	0.16	0.4898	0.0049	2556	25	2562	13	2570	21		−0.54
15LQ08-1-36	136	151	0.90	0.1708	0.0024	11.45	0.14	0.4863	0.0045	2566	23	2561	12	2555	19		0.43
15LQ08-1-37	84	141	0.60	0.1653	0.0023	10.16	0.13	0.4459	0.0041	2511	24	2449	12	2377	18		5.32
15LQ08-1-38	35	257	0.14	0.1642	0.0023	11.34	0.14	0.5009	0.0045	2499	23	2551	12	2618	19		−4.75
	Metamorphic zircon																
15LQ08-1-07	102	849	0.12	0.1646	0.0021	9.26	0.11	0.4083	0.0037	2504	21	2364	11	2207	17		11.85
15LQ08-1-08	90	791	0.11	0.1657	0.0021	9.08	0.10	0.3975	0.0035	2515	21	2346	10	2157	16		14.22
15LQ08-1-09	47	412	0.11	0.1635	0.0020	10.84	0.12	0.4812	0.0042	2492	21	2510	10	2532	18		−1.63
15LQ08-1-11	15	330	0.05	0.1633	0.0021	10.04	0.11	0.4458	0.0039	2490	21	2438	10	2376	18		4.58
15LQ08-1-22	16	531	0.03	0.1634	0.0021	9.99	0.12	0.4434	0.0039	2491	22	2434	11	2366	17		5.03
15LQ08-1-32	24	224	0.10	0.1622	0.0022	10.25	0.13	0.4584	0.0041	2478	23	2457	11	2433	18		1.85

(*continued on next page*)

Table 1 (*continued*)

Spot	Th	U	Th/U	Isotopic ratios						Corrected ages (Ma)							Disc (%)
	(ppm)	(ppm)		$^{207}Pb/^{206}Pb$	1σ	$^{207}Pb/^{235}U$	1σ	$^{206}Pb/^{238}U$	1σ	$^{207}Pb/^{206}Pb$	1σ	$^{207}Pb/^{235}U$	1σ	$^{206}Pb/^{238}U$	1σ		
15LQ08-1-33	17	157	0.11	0.1647	0.0023	10.53	0.13	0.4639	0.0043	2504	23	2483	12	2457	19		1.90
15LQ09-1	Trondhjemitic gneisses																
	Magmatic zircon																
15LQ09-1-02	260	911	0.29	0.1663	0.0020	11.06	0.12	0.4826	0.0042	2521	20	2529	10	2539	18		−0.71
15LQ09-1-06	312	569	0.55	0.1708	0.0020	11.72	0.12	0.4976	0.0043	2566	20	2582	10	2604	19		−1.47
15LQ09-1-07	120	192	0.62	0.1711	0.0021	11.71	0.13	0.4962	0.0045	2569	20	2581	10	2597	19		−1.11
15LQ09-1-09	143	1603	0.09	0.1676	0.0020	11.48	0.12	0.4972	0.0043	2533	20	2563	10	2602	18		−2.70
15LQ09-1-10	133	394	0.34	0.1659	0.0020	10.84	0.12	0.4739	0.0042	2517	20	2510	10	2501	18		0.65
15LQ09-1-11	192	1163	0.17	0.1678	0.0020	11.04	0.12	0.4771	0.0041	2536	20	2527	10	2515	18		0.85
15LQ09-1-12	359	661	0.54	0.1695	0.0020	11.23	0.12	0.4808	0.0042	2553	20	2543	10	2531	18		0.85
15LQ09-1-15	854	987	0.87	0.1699	0.0020	11.44	0.12	0.4887	0.0042	2556	20	2560	10	2565	18		−0.34
15LQ09-1-17	200	943	0.21	0.1662	0.0020	11.08	0.12	0.4836	0.0042	2519	20	2530	10	2543	18		−0.94
15LQ09-1-18	209	1177	0.18	0.1663	0.0020	10.88	0.11	0.4744	0.0041	2521	20	2513	10	2503	18		0.72
15LQ09-1-19	499	803	0.62	0.1713	0.0021	11.57	0.12	0.4901	0.0043	2571	20	2571	10	2571	18		−0.02
15LQ09-1-20	338	1158	0.29	0.1656	0.0020	10.77	0.11	0.4717	0.0041	2514	20	2503	10	2491	18		0.92
15LQ09-1-21	188	830	0.23	0.1682	0.0020	11.18	0.12	0.4823	0.0042	2539	20	2538	10	2537	18		0.08
15LQ09-1-23	218	347	0.63	0.1713	0.0021	11.83	0.13	0.5010	0.0044	2570	20	2591	10	2618	19		−1.87
	Metamorphic zircon																
15LQ09-1-01	60	1208	0.05	0.1654	0.0019	10.97	0.11	0.4811	0.0042	2512	20	2521	10	2532	18		−0.82
15LQ09-1-03	68	1312	0.05	0.1633	0.0019	10.59	0.11	0.4705	0.0041	2490	20	2488	10	2486	18		0.17
15LQ09-1-04	62	1339	0.05	0.1633	0.0019	10.48	0.11	0.4656	0.0040	2490	20	2478	10	2464	18		1.04
15LQ09-1-05	59	1186	0.05	0.1633	0.0019	10.56	0.11	0.4690	0.0041	2490	20	2485	10	2479	18		0.43
15LQ09-1-08	84	1695	0.05	0.1651	0.0019	11.18	0.12	0.4915	0.0042	2508	20	2539	10	2577	18		−2.73
15LQ09-1-13	63	1147	0.05	0.1628	0.0019	10.63	0.11	0.4737	0.0041	2485	20	2491	10	2500	18		−0.59
15LQ09-1-14	62	902	0.07	0.1644	0.0020	10.89	0.11	0.4808	0.0042	2501	20	2514	10	2531	18		−1.20
15LQ09-1-16	33	855	0.04	0.1638	0.0020	10.72	0.11	0.4750	0.0041	2495	20	2500	10	2506	18		−0.42
15LQ09-1-22	44	940	0.05	0.1627	0.0020	10.50	0.11	0.4684	0.0041	2483	20	2480	10	2477	18		0.28
17Sk05	Trondhjemitic gneisses																
	Magmatic zircon																
17SK05-12	84	132	0.64	0.1725	0.0042	11.81	0.30	0.4965	0.0051	2583	40	2590	24	2599	22		−0.60
17SK05-14	286	338	0.84	0.1704	0.0036	11.47	0.25	0.4887	0.0053	2562	35	2562	20	2565	23		−0.11
17SK05-16	119	285	0.42	0.1680	0.0032	11.39	0.20	0.4909	0.0037	2539	32	2556	17	2575	16		−1.41
17SK05-21	157	395	0.40	0.1682	0.0027	11.15	0.17	0.4790	0.0039	2540	27	2536	14	2523	17		0.69
17SK05-29	76	123	0.62	0.1658	0.0028	10.88	0.17	0.4749	0.0036	2517	28	2513	14	2505	16		0.47
17SK05-40	108	152	0.71	0.1693	0.0031	11.09	0.21	0.4764	0.0039	2550	30	2531	18	2511	17		1.52
17SK05-45	45	99	0.46	0.1608	0.0037	10.41	0.26	0.4719	0.0054	2465	39	2472	23	2492	24		−1.10
17SK05-50	210	310	0.68	0.1604	0.0026	10.33	0.16	0.4670	0.0035	2461	28	2465	15	2470	16		−0.38
	Metamorphic zircon																
17SK05-07	158	2197	0.07	0.1649	0.0026	12.76	0.24	0.5605	0.0080	2507	27	2662	18	2869	33		−14.42
17SK05-08	103	1168	0.09	0.1611	0.0027	10.63	0.18	0.4787	0.0047	2478	28	2491	16	2522	21		−1.78
17SK05-09	111	1552	0.07	0.1613	0.0025	11.15	0.18	0.5007	0.0042	2469	26	2535	15	2617	18		−5.96
17SK05-10	270	1553	0.17	0.1614	0.0028	11.70	0.21	0.5251	0.0046	2472	28	2581	17	2721	19		−10.06
17SK05-11	98	1174	0.08	0.1625	0.0032	11.18	0.22	0.4987	0.0036	2481	33	2538	19	2608	15		−5.12
17SK05-13	127	990	0.13	0.1604	0.0037	11.57	0.28	0.5230	0.0050	2461	39	2570	23	2712	21		−10.18
17SK05-15	68	1760	0.04	0.1601	0.0028	11.60	0.21	0.5244	0.0045	2457	30	2572	17	2718	19		−10.61
17SK05-17	240	1018	0.24	0.1628	0.0029	10.97	0.18	0.4867	0.0039	2487	30	2520	15	2556	17		−2.79
17SK05-18	81	1411	0.06	0.1654	0.0029	12.13	0.22	0.5305	0.0063	2522	29	2615	17	2743	26		−8.77
17SK05-19	84	1784	0.05	0.1585	0.0028	10.31	0.20	0.4692	0.0064	2440	30	2463	18	2480	28		−1.64
17SK05-20	72	1225	0.06	0.1618	0.0027	10.44	0.19	0.4653	0.0054	2476	28	2475	17	2463	24		0.52
17SK05-22	135	1288	0.11	0.1566	0.0021	10.98	0.15	0.5054	0.0039	2420	23	2521	13	2637	17		−8.95
17SK05-23	167	304	0.55	0.1572	0.0025	10.91	0.18	0.5007	0.0051	2426	28	2515	15	2617	22		−7.89

(*continued on next page*)

Table 1 (*continued*)

Spot	Th	U	Th/U	Isotopic ratios					Corrected ages (Ma)							Disc (%)
	(ppm)	(ppm)		$^{207}Pb/^{206}Pb$	1σ	$^{207}Pb/^{235}U$	1σ	$^{206}Pb/^{238}U$	1σ	$^{207}Pb/^{206}Pb$	1σ	$^{207}Pb/^{235}U$	1σ	$^{206}Pb/^{238}U$	1σ	
17SK05-24	127	1422	0.09	0.1570	0.0025	11.10	0.16	0.5105	0.0043	2424	27	2532	14	2659	18	−9.69
17SK05-26	139	1915	0.07	0.1585	0.0023	11.28	0.16	0.5142	0.0047	2440	24	2547	14	2674	20	−9.61
17SK05-27	103	1775	0.06	0.1553	0.0022	9.45	0.15	0.4391	0.0047	2406	23	2383	15	2347	21	2.45
17SK05-28	136	3369	0.04	0.1611	0.0025	10.87	0.21	0.4884	0.0086	2478	27	2512	18	2564	37	−3.48
17SK05-30	116	1292	0.09	0.1573	0.0025	11.28	0.18	0.5178	0.0045	2428	27	2546	15	2690	19	−10.80
17SK05-31	238	1516	0.16	0.1629	0.0026	11.95	0.20	0.5301	0.0054	2487	32	2601	16	2742	23	−10.25
17SK05-32	262	1511	0.17	0.1613	0.0023	11.44	0.17	0.5125	0.0044	2469	19	2560	14	2667	19	−8.02
17SK05-33	143	2019	0.07	0.1612	0.0026	7.89	0.21	0.3527	0.0074	2468	27	2218	24	1947	35	21.10
17SK05-34	454	3546	0.13	0.1652	0.0022	12.39	0.18	0.5410	0.0046	2510	22	2634	14	2787	19	−11.07
17SK05-35	78	2265	0.03	0.1637	0.0025	10.82	0.17	0.4769	0.0044	2495	26	2508	15	2514	19	−0.75
17SK05-37	148	1497	0.10	0.1614	0.0030	8.86	0.17	0.3972	0.0050	2472	31	2324	18	2156	23	12.78
17SK05-38	73	1385	0.05	0.1620	0.0026	11.81	0.21	0.5276	0.0061	2476	27	2589	16	2731	26	−10.31
17SK05-39	129	1468	0.09	0.1582	0.0025	10.15	0.17	0.4658	0.0044	2436	27	2449	15	2465	19	−1.20
17SK05-42	58	2504	0.02	0.1587	0.0034	11.25	0.27	0.5163	0.0057	2442	36	2544	23	2683	24	−9.87
17SK05-43	165	1670	0.10	0.1600	0.0036	11.42	0.29	0.5207	0.0056	2457	38	2558	24	2702	24	−9.97
17SK05-44	2	132	0.01	0.1624	0.0049	10.94	0.27	0.4968	0.0051	2481	51	2518	23	2600	22	−4.81
17SK05-46	169	232	0.73	0.1631	0.0031	10.86	0.22	0.4847	0.0043	2488	31	2511	19	2548	19	−2.39
17SK05-48	155	1003	0.15	0.1601	0.0026	11.94	0.20	0.5414	0.0045	2457	27	2600	16	2789	19	−13.51
	Later-thermal-event zircon															
17SK05-01	92	1493	0.06	0.1417	0.0067	8.95	0.68	0.4920	0.0076	2250	82	2332	69	2579	33	−14.63
17SK05-02	171	337	0.51	0.1489	0.0059	9.63	0.59	0.4972	0.0073	2344	68	2400	57	2602	32	−10.97
17SK05-03	248	1567	0.16	0.1509	0.0048	10.79	0.52	0.5419	0.0068	2367	54	2505	45	2792	29	−17.95
17SK05-04	186	1062	0.18	0.1498	0.0037	9.78	0.35	0.4888	0.0050	2344	42	2414	33	2565	22	−9.47
17SK05-05	102	2298	0.04	0.1534	0.0030	7.82	0.21	0.3771	0.0051	2384	33	2211	25	2063	24	13.49
17SK05-25	144	969	0.15	0.1547	0.0027	10.06	0.17	0.4695	0.0056	2399	29	2441	16	2481	25	−3.43
17SK05-36	102	1329	0.08	0.1527	0.0026	7.81	0.16	0.3685	0.0049	2376	29	2209	18	2022	23	14.90
17SK05-41	80	3062	0.03	0.1559	0.0030	8.57	0.20	0.4000	0.0055	2413	28	2294	21	2169	25	10.11
17SK05-47	173	1201	0.14	0.1559	0.0027	11.07	0.20	0.5160	0.0039	2413	29	2529	17	2682	17	−11.16
17SK05-49	142	1296	0.11	0.1540	0.0024	8.68	0.14	0.4087	0.0030	2391	26	2305	14	2209	14	7.61

Notes: Degree of discordance = 100×(1−($^{206}Pb/^{238}U$ age/$^{207}Pb/^{206}Pb$ age)), $\lambda^{238}U = 0.0155125 \times 10^{-9}$ yr^{-1}, $\lambda^{235}U = 0.98485 \times 10^{-9}$ yr^{-1}, $\lambda^{232}Th = 0.049475 \times 10^{-9}$ yr^{-}.

Table 2
Zircon Hf-O isotopic data.

No.	*t*(Ma)	$^{176}Yb/^{177}Hf$	$^{176}Lu/^{177}Hf$	$^{176}Hf/^{177}Hf$	±2σ	$\varepsilon_{Hf}(t)$	2σ	T_{DM}	$T_{DM}(Hf)^{C}$	2σ	$T_{DM}(Hf2)$	$f_{Lu/Hf}$	$\delta^{18}O$ (‰, VSMOW)	±2σ (internal)	±2σ (external)
15LQ07-1	Dioritic gneiss														
	Magmatic zircon														
15LQ07-1-01	2606	0.018348	0.000650	0.281370	0.000009	9.0	1.7	2604	2602	16	2601	−0.98			
15LQ07-1-02	2621	0.019327	0.000804	0.281381	0.000011	8.3	0.7	2599	2586	16	2571	−0.98			
15LQ07-1-03	2589	0.019460	0.000710	0.281376	0.000010	7.6	0.3	2599	2606	13	2613	−0.98			
15LQ07-1-04	2580	0.027738	0.000917	0.281348	0.000012	6.0	0.4	2651	2694	16	2741	−0.97			
15LQ07-1-06	2502	0.008593	0.000354	0.281409	0.000011	7.4	0.4	2530	2548	15	2568	−0.99			
15LQ07-1-07	2487	0.013918	0.000542	0.281384	0.000010	5.8	0.4	2577	2632	14	2693	−0.98			
15LQ07-1-08	2573	0.026844	0.000973	0.281373	0.000013	6.7	0.5	2620	2649	17	2680	−0.97			
15LQ07-1-09	2524	0.035351	0.001194	0.281406	0.000016	6.3	0.6	2591	2631	22	2675	−0.96			
15LQ07-1-10	2503	0.019536	0.000730	0.281343	0.000009	4.4	0.3	2645	2733	12	2829	−0.98			
15LQ07-1-12	2435	0.026080	0.000905	0.281400	0.000013	4.6	0.5	2580	2667	18	2764	−0.97			
15LQ07-1-13	2498	0.021278	0.000773	0.281403	0.000010	6.4	0.3	2567	2609	13	2655	−0.98			
15LQ07-1-14	2443	0.010977	0.000458	0.281374	0.000012	4.6	0.4	2584	2673	17	2769	−0.99			
15LQ07-1-16	2442	0.019378	0.000769	0.281363	0.000013	3.7	0.5	2620	2729	17	2849	−0.98			
15LQ07-1-17	2479	0.027788	0.001113	0.281389	0.000013	4.9	0.5	2609	2686	18	2773	−0.97			
15LQ07-1-19	2471	0.025487	0.000872	0.281371	0.000010	4.5	0.3	2616	2704	13	2801	−0.97			
15LQ07-1-20	2454	0.037680	0.001248	0.281374	0.000013	3.5	0.5	2639	2748	18	2871	−0.96			
15LQ07-1-21	2539	0.019759	0.000664	0.281362	0.000010	6.0	0.4	2615	2661	14	2712	−0.98			
15LQ07-1-24	2494	0.013146	0.000506	0.281378	0.000010	5.9	0.4	2583	2637	14	2697	−0.98			
15LQ07-1-26	2554	0.023015	0.000796	0.281366	0.000009	6.3	0.3	2618	2657	12	2701	−0.98			
15LQ07-1-27	2557	0.048073	0.001593	0.281392	0.000012	5.9	0.4	2638	2684	16	2737	−0.95			
15LQ07-1-28	2539	0.031861	0.001045	0.281361	0.000013	5.3	0.5	2642	2704	18	2774	−0.97			
15LQ07-1-30	2576	0.031536	0.001037	0.281369	0.000013	6.5	0.4	2630	2663	17	2699	−0.97			
15LQ07-1-31	2554	0.034743	0.001157	0.281367	0.000010	5.7	0.4	2642	2695	14	2754	−0.97			
15LQ07-1-34	2494	0.045858	0.001491	0.281383	0.000011	4.4	0.4	2643	2728	15	2826	−0.96			
15LQ07-1-35	2559	0.015807	0.000575	0.281376	0.000009	7.1	0.3	2590	2610	12	2631	−0.98			
15LQ07-1-36	2587	0.015133	0.000549	0.281363	0.000010	7.4	0.3	2606	2618	13	2630	−0.98			
15LQ07-1-37	2595	0.018036	0.000642	0.281343	0.000016	6.7	0.6	2638	2665	21	2695	−0.98			
15LQ07-1-38	2581	0.049150	0.001591	0.281412	0.000011	7.1	0.4	2610	2627	16	2646	−0.95			
15LQ07-1-39	2479	0.015466	0.000551	0.281343	0.000011	4.2	0.4	2633	2728	15	2832	−0.98			
15LQ07-1-40	2544	0.029908	0.001207	0.281355	0.000016	5.0	0.6	2661	2730	22	2809	−0.96			
15LQ07-1-42	2502	0.033600	0.001124	0.281377	0.000011	4.9	0.4	2626	2700	15	2783	−0.97			
15LQ07-1-43	2511	0.019354	0.000726	0.281373	0.000010	5.7	0.4	2605	2662	13	2726	−0.98			
15LQ07-1-44	2587	0.044829	0.001425	0.281401	0.000012	7.2	0.4	2614	2629	17	2647	−0.96			
15LQ07-1-47	2461	0.026793	0.000889	0.281353	0.000012	3.6	0.4	2642	2751	17	2873	−0.97			
15LQ07-1-48	2472	0.024513	0.000820	0.281358	0.000012	4.1	0.4	2631	2727	17	2834	−0.98			
15LQ07-1-51	2450	0.009937	0.000421	0.281380	0.000014	5.0	0.5	2575	2653	18	2738	−0.99			
15LQ07-1-53	2431	0.036699	0.001184	0.281394	0.000013	3.9	0.4	2606	2710	17	2827	−0.96			
15LQ07-1-54	2535	0.027672	0.000908	0.281372	0.000010	5.9	0.3	2619	2669	13	2724	−0.97			
15LQ07-1-55	2492	0.028453	0.000935	0.281361	0.000013	4.5	0.5	2634	2720	18	2815	−0.97			
15LQ07-1-56	2473	0.024689	0.000856	0.281368	0.000013	4.4	0.5	2620	2708	18	2807	−0.97			
15LQ07-1-58	2495	0.019359	0.000764	0.281371	0.000010	5.2	0.4	2609	2678	14	2755	−0.98			
15LQ07-1-59	2527	0.004930	0.000224	0.281357	0.000010	6.3	0.3	2592	2633	13	2677	−0.99			
15LQ07-1-60	2528	0.032306	0.001301	0.281374	0.000010	5.1	0.3	2642	2709	14	2785	−0.96			
	Metamorphic zircon														
15LQ07-1-05	2490	0.014538	0.000575	0.281397	0.000010	6.3	0.4	2562	2607	13	2655	−0.98			
15LQ07-1-11	2473	0.010574	0.000430	0.281404	0.000014	6.4	0.5	2542	2585	18	2633	−0.99			
15LQ07-1-15	2455	0.007095	0.000299	0.281375	0.000012	5.2	0.4	2573	2648	16	2729	−0.99			
15LQ07-1-22	2413	0.007470	0.000304	0.281393	0.000010	4.9	0.3	2549	2634	13	2726	−0.99			
15LQ07-1-23	2427	0.008799	0.000364	0.281382	0.000010	4.7	0.4	2568	2655	13	2751	−0.99			
15LQ07-1-25	2478	0.007828	0.000330	0.281382	0.000010	5.9	0.4	2566	2621	14	2682	−0.99			
15LQ07-1-29	2479	0.010158	0.000413	0.281370	0.000010	5.4	0.4	2587	2654	14	2727	−0.99			

(*continued on next page*)

Table 2 (*continued*)

No.	*t*(Ma)	$^{176}Yb/^{177}Hf$	$^{176}Lu/^{177}Hf$	$^{176}Hf/^{177}Hf$	±2σ	$\varepsilon_{Hf}(t)$	2σ	T_{DM}	$T_{DM}(Hf)^C$	2σ	$T_{DM}(Hf2)$	$f_{Lu/Hf}$	$\delta^{18}O$ (‰, VSMOW)	±2σ (internal)	±2σ (external)
15LQ07-1-32	2454	0.010601	0.000435	0.281414	0.000011	6.3	0.4	2530	2577	15	2628	−0.99			
15LQ07-1-33	2457	0.021211	0.000716	0.281362	0.000010	4.1	0.4	2618	2716	14	2825	−0.98			
15LQ07-1-41	2502	0.028008	0.000949	0.281362	0.000011	4.7	0.4	2635	2715	15	2804	−0.97			
15LQ07-1-45	2442	0.009299	0.000382	0.281372	0.000009	4.7	0.3	2583	2671	13	2766	−0.99			
15LQ07-1-46	2432	0.008662	0.000342	0.281373	0.000010	4.5	0.3	2578	2670	13	2770	−0.99			
	Later-thermal-event zircon														
15LQ07-1-18	2387	0.017126	0.000599	0.281370	0.000010	3.0	0.4	2600	2731	13	2875	−0.98			
15LQ07-1-49	2381	0.011951	0.000506	0.281393	0.000011	3.8	0.4	2563	2676	15	2799	−0.98			
15LQ07-1-50	2396	0.012770	0.000543	0.281397	0.000011	4.2	0.4	2559	2660	14	2771	−0.98			
15LQ07-1-52	2386	0.007559	0.000350	0.281408	0.000016	4.7	0.6	2532	2623	21	2722	−0.99			
15LQ07-1-57	2395	0.005164	0.000259	0.281380	0.000013	4.1	0.5	2564	2670	18	2786	−0.99			
15LQ08-1	Tonalitic gneiss														
	Magmatic zircon														
15LQ08-1-01	2529	0.049676	0.001499	0.281390	0.000021	5.4	0.8	2633	2694	29	2763	−0.95			
15LQ08-1-02	2574	0.043584	0.001333	0.281388	0.000023	6.6	0.8	2625	2655	31	2689	−0.96			
15LQ08-1-03	2574	0.026082	0.000811	0.281357	0.000021	6.4	0.8	2632	2667	29	2707	−0.98			
15LQ08-1-04	2590	0.042341	0.001350	0.281434	0.000019	8.6	0.7	2562	2546	26	2528	−0.96			
15LQ08-1-05	2551	0.058803	0.001775	0.281426	0.000027	6.7	1.0	2603	2632	38	2666	−0.95			
15LQ08-1-06	2540	0.035000	0.001143	0.281402	0.000021	6.6	0.7	2593	2625	28	2661	−0.97			
15LQ08-1-10	2583	0.060501	0.001831	0.281451	0.000025	8.1	0.9	2573	2567	34	2560	−0.94			
15LQ08-1-12	2566	0.024854	0.000841	0.281408	0.000020	8.0	0.7	2564	2563	28	2562	−0.97			
15LQ08-1-13	2563	0.114201	0.003388	0.281465	0.000024	5.5	0.9	2663	2712	35	2775	−0.90			
15LQ08-1-14	2571	0.047446	0.001457	0.281391	0.000021	6.4	0.7	2630	2664	29	2703	−0.96			
15LQ08-1-15	2577	0.062862	0.001899	0.281478	0.000023	8.8	0.8	2540	2519	33	2494	−0.94			
15LQ08-1-16	2541	0.049334	0.001538	0.281410	0.000023	6.3	0.8	2608	2647	31	2692	−0.95			
15LQ08-1-17	2545	0.051190	0.001622	0.281388	0.000024	5.4	0.9	2646	2703	34	2770	−0.95			
15LQ08-1-18	2564	0.047541	0.001517	0.281378	0.000022	5.7	0.8	2651	2701	31	2759	−0.95			
15LQ08-1-19	2518	0.029718	0.000951	0.281375	0.000020	5.5	0.7	2616	2676	27	2742	−0.97			
15LQ08-1-20	2553	0.070716	0.002158	0.281444	0.000024	6.7	0.8	2604	2632	33	2665	−0.94			
15LQ08-1-21	2564	0.066331	0.002057	0.281371	0.000022	4.5	0.8	2700	2775	31	2864	−0.94			
15LQ08-1-23	2579	0.048593	0.001503	0.281467	0.000021	9.2	0.8	2527	2497	30	2463	−0.95			
15LQ08-1-24	2545	0.020311	0.000672	0.281386	0.000019	7.0	0.7	2582	2605	26	2630	−0.98			
15LQ08-1-25	2558	0.069489	0.002187	0.281474	0.000021	7.8	0.7	2564	2567	30	2571	−0.93			
15LQ08-1-26	2566	0.060440	0.001820	0.281476	0.000021	8.7	0.7	2536	2520	29	2500	−0.95			
15LQ08-1-27	2559	0.051930	0.001646	0.281407	0.000026	6.4	0.9	2620	2655	36	2695	−0.95			
15LQ08-1-28	2570	0.076721	0.002315	0.281452	0.000028	7.0	1.0	2605	2623	39	2646	−0.93			
15LQ08-1-29	2557	0.048800	0.001500	0.281438	0.000024	7.7	0.9	2568	2574	33	2581	−0.95			
15LQ08-1-30	2540	0.051624	0.001847	0.281459	0.000025	7.4	0.9	2563	2576	36	2591	−0.94			
15LQ08-1-31	2559	0.063833	0.001962	0.281426	0.000022	6.5	0.8	2616	2648	30	2686	−0.94			
15LQ08-1-34	2594	0.027023	0.000898	0.281331	0.000020	5.8	0.7	2673	2721	27	2774	−0.97			
15LQ08-1-35	2556	0.051109	0.001595	0.281453	0.000021	8.0	0.7	2554	2553	29	2551	−0.95			
15LQ08-1-36	2566	0.114068	0.003468	0.281520	0.000025	7.4	0.9	2589	2600	36	2615	−0.90			
15LQ08-1-37	2511	0.040089	0.001339	0.281345	0.000021	3.6	0.8	2685	2787	29	2903	−0.96			
15LQ08-1-38	2499	0.038033	0.001192	0.281388	0.000021	5.2	0.7	2615	2684	28	2761	−0.96			
	Metamorphic zircon														
15LQ08-1-07	2504	0.039793	0.001527	0.281459	0.000024	7.2	0.9	2540	2561	34	2586	−0.95			
15LQ08-1-08	2515	0.091508	0.002774	0.281534	0.000025	8.0	0.9	2519	2522	35	2525	−0.92			
15LQ08-1-09	2492	0.024168	0.000824	0.281430	0.000024	7.1	0.8	2533	2558	32	2585	−0.98			
15LQ08-1-11	2490	0.028135	0.000898	0.281378	0.000019	5.1	0.7	2609	2681	26	2761	−0.97			
15LQ08-1-22	2491	0.047727	0.001433	0.281382	0.000022	4.4	0.8	2640	2727	30	2825	−0.96			
15LQ08-1-32	2478	0.049175	0.001581	0.281434	0.000024	5.7	0.8	2578	2635	33	2701	−0.95			
15LQ08-1-33	2504	0.034798	0.001131	0.281398	0.000024	5.7	0.9	2598	2654	33	2716	−0.97			
15LQ09-1	Trondhjemitic gneiss														

(*continued on next page*)

Table 2 (*continued*)

No.	t(Ma)	$^{176}Yb/^{177}Hf$	$^{176}Lu/^{177}Hf$	$^{176}Hf/^{177}Hf$	±2σ	$\varepsilon_{Hf}(t)$	2σ	T_{DM}	$T_{DM}(Hf)^{C}$	2σ	$T_{DM}(Hf2)$	$f_{Lu/Hf}$	$\delta^{18}O$ (‰, VSMOW)	±2σ (internal)	±2σ (external)
Magmatic zircon															
15LQ09-1-02	2521	0.073201	0.002107	0.281452	0.000018	6.3	0.6	2590	2628	25	2673	−0.94	6.54	0.21	0.70
15LQ09-1-06	2566	0.091487	0.002698	0.281521	0.000021	8.8	0.8	2533	2515	30	2494	−0.92	6.15	0.49	0.83
15LQ09-1-07	2569	0.102583	0.003088	0.281498	0.000029	7.3	1.0	2593	2606	41	2621	−0.91	6.36	0.46	0.81
15LQ09-1-09	2533	0.065588	0.002123	0.281472	0.000015	7.3	0.5	2563	2579	21	2597	−0.94	5.98	0.39	0.78
15LQ09-1-10	2517	0.068954	0.002058	0.281458	0.000021	6.6	0.8	2578	2612	30	2651	−0.94	6.96	0.44	0.80
15LQ09-1-11	2536	0.074746	0.002201	0.281429	0.000017	5.7	0.6	2629	2680	23	2740	−0.93	6.15	0.35	0.76
15LQ09-1-12	2553	0.089810	0.002630	0.281492	0.000018	7.5	0.6	2570	2579	26	2590	−0.92	7.87	0.18	0.70
15LQ09-1-15	2556	0.076818	0.002356	0.281487	0.000020	7.9	0.7	2558	2558	28	2559	−0.93	7.04	0.42	0.79
15LQ09-1-17	2519	0.091494	0.002676	0.281479	0.000021	6.3	0.7	2592	2630	29	2676	−0.92	6.87	0.11	0.68
15LQ09-1-18	2521	0.064944	0.001944	0.281425	0.000019	5.6	0.7	2617	2671	27	2733	−0.94	7.72	0.19	0.70
15LQ09-1-19	2571	0.065635	0.001945	0.281428	0.000016	6.8	0.6	2613	2636	23	2663	−0.94	7.31	0.30	0.74
15LQ09-1-20	2514	0.092796	0.002761	0.281435	0.000022	4.5	0.8	2661	2737	31	2831	−0.92	6.86	0.25	0.72
15LQ09-1-21	2539	0.077261	0.002298	0.281446	0.000019	6.2	0.7	2612	2652	27	2699	−0.93	7.05	0.05	0.67
15LQ09-1-23	2570	0.084314	0.002511	0.281530	0.000023	9.5	0.8	2507	2474	32	2434	−0.92	7.44	0.20	0.70
Metamorphic zircon															
15LQ09-1-01	2512	0.035740	0.001200	0.281403	0.000014	5.9	0.5	2595	2645	19	2701	−0.96	5.84	0.69	0.96
15LQ09-1-03	2490	0.030746	0.001061	0.281397	0.000016	5.5	0.6	2594	2657	21	2726	−0.97	5.92	0.21	0.70
15LQ09-1-04	2490	0.036720	0.001283	0.281424	0.000012	6.1	0.4	2572	2621	17	2675	−0.96	5.69	0.28	0.73
15LQ09-1-05	2490	0.024844	0.000914	0.281367	0.000019	4.7	0.7	2625	2706	26	2796	−0.97	3.78	0.19	0.70
15LQ09-1-08	2508	0.071101	0.002585	0.281469	0.000017	5.9	0.6	2599	2647	24	2706	−0.92	5.08	0.19	0.70
15LQ09-1-13	2485	0.028816	0.001022	0.281390	0.000017	5.2	0.6	2602	2671	23	2749	−0.97	4.96	0.76	1.01
15LQ09-1-14	2501	0.041904	0.001411	0.281418	0.000011	5.9	0.4	2589	2641	15	2700	−0.96			
15LQ09-1-16	2495	0.020323	0.000689	0.281366	0.000016	5.1	0.6	2612	2683	22	2761	−0.98			
15LQ09-1-22	2483	0.024803	0.000821	0.281397	0.000018	5.7	0.6	2578	2636	24	2699	−0.98			

Though most boundaries between the granitoid gneisses and supracrustal sequences are unclear, the TTG gneisses at Xiaolaihe area are in fault contact with the supracrustal rocks. Zircon U–Pb dating by sensitive high resolution ion microprobe (SHRIMP) and laser ablation–inductively coupled plasma–mass spectrometry (LA–ICP–MS) instruments revealed that the majority of the Qingyuan granite–greenstone terrain were formed at the end of the Neoarchean between 2.51 and 2.56 Ga and subsequently subjected to high amphibolite- to granulite-facies metamorphism (Bai et al., 2014; Grant et al., 2009; Li and Wei, 2017; Wan et al., 2005a; Wang et al., 2016a, 2016b; Wu et al., 2016; this paper), indicative of a synchronism between the granitoid gneisses and supracrustal sequences. The granitoid gneisses consist of predominant TTG and subordinate potassic granitoid (monzogranite and syenogranite), with minor diorite in precursor. The supracrustal sequences occur as intercalated successions or xenoliths within the gneisses (Bai et al., 2014; Li and Wei, 2017; Peng et al., 2015; Wang et al., 2016b), which was subdivided into the Shipengzi, Hongtoushan and Nantianmen formations from bottom to top (Zhai et al., 1985). Specifically, the lowermost Shipengzi and Hongtoushan formations consist predominantly of komatiite, tholeiite and andesite in precursor, preserved as amphibolite, pyroxene hornblendite, and biotite–plagioclase and sillimanite- or kyanite-bearing gneiss (Li and Wei, 2017; Peng et al., 2015; Zhai et al., 1985). The Nantianmen Formation is composed of biotite–plagioclase gneiss, muscovite–biotite–quartz–schist, amphibolite, magnetite–quartzite, banded iron formation and marble (Peng et al., 2015; Wan et al., 2005a; Zhai et al., 1985).

In this contribution, we focus on the nineteen granitoid gneisses at Qingyuan area in northern Liaoning, North China Craton (GPS location: 42°04′22″N, 129°36′25″E, Height: 330 m; Fig. 1B). They have undergone intense metamorphism and deformation with a mineral preferred orientation (Fig. 2). The TTG gneisses show medium- to coarse-grained granoblastic textures and strongly gneissic structures, whereas the dioritic gneisses show fine-grained granoblastic textures and weakly gneissic to massive structures (Fig. 2). The dioritic gneisses occur in form of dykes, enclaves, or intercalated within the TTG gneisses (Fig. 2A–F). The TTG gneisses contain plagioclase (45–55%), quartz (25–30%), hornblende (5–15%), biotite (0–10%), K-feldspar (5–10%), and garnet (0–3%), along with accessory zircon, apatite, titanite, and magnetite (Fig. 2 G–H). The dioritic gneisses are composed primarily of plagioclase (45%–60%), hornblende (20%–30%), quartz (5–10%), biotite (0–5%), pyroxene (0–5%), garnet (0–3%), and K-feldspar (0–3%) (Fig. 2I).

3. Analytical methods

Data acquisition and results for the granitoid gneisses at Qingyuan area in northern Liaoning are presented in detail as Supplemental File 1 and Tables 1–4, including zircon U–Pb isotope measurements using LA–ICP–MS at the Wuhan Sample Solution Analytical Technology Co., Ltd, Wuhan, zircon O isotope analyses using SHRIMP stable isotope (SHRIMP SI) ion microprobe at the Research School of Earth Sciences, Australian National University, Canberra, zircon Lu–Hf isotope measurements using LA–multi-collector (MC) –ICP–MS at the Wuhan Sample Solution Analytical Technology Co., Ltd, whole-rock major element analyses using X-ray fluorescence spectrometry (XRF) at the Geoanalytical Center of Nuclear Industry, Beijing, whole-rock trace element analyses using ICP–MS at Geological Laboratory Center in the China University of Geosciences, Beijing, whole-rock Sm–Nd isotope measurements using a Thermo-Finnigan TRITON thermal ionisation mass spectrometer (TIMS) at the Isotope Laboratory in the Institute of Geology and Mineral Resources, China Geological Survey, Tianjin, and whole-rock oxygen isotope measurements using a MAT-252 mass spectrometer at the Geoanalytical Center of Nuclear Industry, Beijing. Detailed procedures and instrument parameters can be seen in Supplemental File 1.

Table 3
Whole-rock Nd and O isotope compositions.

Sample No.	Sm (ppm)	Nd (ppm)	$^{147}Sm/^{144}Nd$	$^{143}Nd/^{144}Nd$	2σ	$\varepsilon_{Nd}(0)$	$f_{Sm/Nd}$	$\varepsilon_{Nd}(T)$ (2500 Ma)	T_{DM} (Ga)	$\delta^{18}O$ (‰)	Calculated zircon $\delta^{18}O$ (‰)
Trondhjemitic gneisses											
17SK05	2.43	13.70	0.1072	0.511232	5	−27.4	−0.45	1.1	2.7		
15Q-9-1	0.14	1.16	0.0719	0.510844	16	−35.0	−0.63	4.8	2.5	8.4	5.6
LQ6-10	2.51	18.90	0.0803	0.510836	1	−35.2	−0.59	2.0	2.6		
LQ9-7	1.76	18.90	0.0563	0.510384	2	−44.0	−0.71	0.8	2.7		
Tonalitic gneiss											
15Q-8-1	3.07	12.70	0.1461	0.512086	5	−10.8	−0.26	5.4	2.4	8.6	7.0
15Q-9-2	1.80	13.40	0.0812	0.510856	4	−34.8	−0.59	2.1	2.6	8.5	6.0
15Q-13	2.20	13.70	0.0971	0.511165	10	−28.7	−0.51	3.0	2.6	9.8	8.3
Granodioritic gneiss											
LQ1-6	4.86	30.30	0.0970	0.511158	2	−28.9	−0.51	2.9	2.6		
LQ5-5	5.65	34.9	0.0979	0.511093	14	−30.1	−0.50	1.4	2.7		
LQ6-2	1.59	8.32	0.1155	0.511521	2	−21.8	−0.41	4.1	2.5		
Dioritic gneiss											
15Q-7-1	2.76	11.30	0.1477	0.512099	6	−10.5	−0.25	5.1	2.4	8.0	6.6
15Q-7-2	4.98	21.60	0.1394	0.511908	6	−14.2	−0.29	4.0	2.5	7.5	6.4
15Q-8-2	8.32	40.40	0.1245	0.511626	3	−19.7	−0.37	3.3	2.6	10.9	10.3

Note: $\varepsilon_{Nd} = (((^{143}Nd/^{144}Nd)_s/(^{143}Nd/^{144}Nd)_{CHUR} - 1) \times 10000$, $f_{Sm/Nd} = (^{147}Sm/^{144}Nd)_s/(^{147}Sm/^{144}Nd)_{CHUR} - 1$, $(^{143}Nd/^{144}Nd)_{CHUR} = 0.512638$, and $(^{147}Sm/^{144}Sm)_{CHUR} = 0.1967$. The model ages were calculated using a linear isotopic ratio growth equation: $T_{DM} = 1/l \times \ln(1 + ((^{143}Nd/^{144}Nd)_s - 0.51315)/((^{147}Sm/^{144}Nd)_s - 0.2137))$.

4. Results

4.1. Zircon U–Pb geochronology

The CL images of representative zircons from the granitoid gneisses in northern Liaoning (Fig. 3) provide constrains on the genesis of the zircons, e.g., magmatic or metamorphic origin. Most zircons commonly have core–rim structures in the CL images and are subhedral to euhedral columnar, with long axes of 80–200 μm in length. The cores of medium CL response show oscillatory growth zoning and striped absorption, both indicative of a magmatic origin (Belousova et al., 2002; Corfu et al., 2003). In comparison, the dark rims (except spot #29 from sample 15LQ07-1; Fig. 3A) have blurred irregular banding and zoning, indicative of recrystallization during metamorphism (Boniface et al., 2012; Corfu et al., 2003; Dubińska et al., 2004; Tomaschek, 2003), despite the metamorphic rims of variable widths (Fig. 3). Zircons of none core–rim structures are rounded to subhedral columnar in shape (e.g., spot #23 from sample 15LQ07-1 in Fig. 3A). However, they share a similarly dark color, blurred zoning or banded zoning with the aforementioned metamorphic rims, indicating a metamorphic origin (Fig. 3A). The red, green and grey solid circles in the CL images represent analytical sites of the magmatic, metamorphic and later-thermal-event domains of zircons, respectively. Besides the CL images, the magmatic and metamorphic zircons have different characteristics in other aspects. (i) Th/U ratios of the magmatic zircons (generally > 0.4) have higher than those of the metamorphic ones (mostly < 0.1) (Table 1). (ii) As is always the case, the metamorphic zircons yield $^{207}Pb/^{206}Pb$ ages slightly younger than 2.5 Ga, while the magmatic zircons generally have older ages (>2.5 Ga) (Table 1). (iii) In addition, the magmatic zircons possess higher rare earth elements (REEs) contents in comparison with the metamorphic zircons, especially the heavy REEs (Supplemental File 2). The ancient zircons have been affected by later thermal events, as recorded in the younger zircons with ages ranging from 2.4 to 2.2 Ga (Fig. 4A, D; Table 1), which has been reported in the vicinity (e.g., Li et al., 2019c). Some U–Pb age data are reverse discordant possibly due to recrystallization overprints of later thermal events and/or the cracks resulting from radioactive damage in the zircons.

4.1.1. Dioritic gneiss

Sixty analyses were obtained from sample 15LQ07-1. The magmatic zircon cores have Th of 14–498 ppm (62 ppm on average) and U of 27–589 ppm (98 ppm on average), yielding Th/U ratios of 0.21–1.22 (0.69 on average). The core analyses define an upper intercept age of 2521 ± 19 Ma (the mean square weighted deviation (MSWD) = 2.2, n = 43), which is consistent with the weighted mean $^{207}Pb/^{206}Pb$ age of 2519 ± 13 Ma (2431–2621 Ma; MSWD = 1.6, n = 43; Fig. 4A). The metamorphic rims contain Th of 7–59 ppm (34 ppm on average) and U of 23–293 ppm (147 ppm on average), yielding much lower average Th/U ratio of 0.24 than that of the magmatic cores. A few metamorphic rims share slightly high Th/U ratios (>0.1), possibly due to inheritance from magmatic zones with extremely high Th/U ratios, and/or dissolution of Th-rich accessory minerals (such as monazite; Li et al., 2020). The rim analyses define an upper intercept age of 2473 ± 16 Ma (MSWD = 0.3, n = 12) and give a weighted mean $^{207}Pb/^{206}Pb$ age of 2457 ± 21 Ma (2413–2502 Ma; MS WD = 0.6, n = 12; Fig. 4A). Five analyses on the outer rims yield a weighted mean $^{207}Pb/^{206}Pb$ age of 2389 ± 20 Ma (MSWD = 0.1), representing a later thermal event.

4.1.2. Tonalitic gneiss

Thirty-eight analyses were obtained from sample 15LQ08-1. The magmatic cores have Th of 16–162 ppm (55 ppm on average) and U of 43–303 ppm (114 ppm on average), yielding Th/U ratios of 0.12–0.92 (0.52 on average). The core analyses define an upper intercept age of 2557 ± 10 Ma (MSWD = 1.2, n = 31), which is consistent with the weighted mean $^{207}Pb/^{206}Pb$ age of 2556 ± 4 Ma (2499–2594 Ma; MSWD = 3.6, n = 31; Fig. 4B). The metamorphic rims contain Th of 15–102 ppm (44 ppm on average) and U of 157–849 ppm (471 ppm on average), yielding relatively low Th/U ratios (0.03–0.12, 0.09 on average). The rim analyses define an upper intercept age of 2491 ± 18 Ma (MSWD = 0.3, n = 7) and give a weighted mean $^{207}Pb/^{206}Pb$ age of 2473 ± 12 Ma (2478–2515 Ma; MSWD = 1.2, n = 7; Fig. 4B).

4.1.3. Trondhjemitic gneiss

Thirty-three analyses were obtained from sample 15LQ09-1. The magmatic zircon cores have Th of 120–854 ppm (288 ppm on average) and U of 192–1602 ppm (838 ppm on average), yielding slightly high Th/U ratios (0.09–0.87, 0.40 on average). The core analyses define an upper intercept age of 2534 ± 23 Ma (MSWD = 0.5, n = 14), which is comparable with the weighted mean $^{207}Pb/^{206}Pb$ age of 2542 ± 5 Ma (2514–2571 Ma; MSWD = 4.7, n = 14; Fig. 4C). The metamorphic rims contain Th of 33–84 ppm (60 ppm on average) and U of 855–1695 ppm (1176 ppm on average), yielding relatively low Th/U ratios (0.04–0.07,

Table 4
. Chemical data.

	Trondhjemitic gneisses							Tonalitic gneisses				Granodioritic gneisses				Dioritic gneisses			
No.	15SK05	LQ6-6	LQ6-10	LQ9-6	LQ9-7	15LQ-9-1	15Q-24-3	LQ6-5	15LQ-8-1	15LQ-9-2	15Q-13	LQ1-6	LQ5-5	LQ6-2	LQ6-3	LQ4-6	15LQ-7-1	15LQ-7-2	15LQ-8-2
(wt.%)																			
SiO_2	72.37	74.34	68.17	72.02	70.70	86.46	70.51	69.27	66.96	81.26	64.72	65.06	66.79	67.23	69.38	61.19	63.37	59.23	50.91
TiO_2	0.15	0.04	0.32	0.30	0.34	0.06	0.28	0.38	0.29	0.06	0.42	0.54	0.50	0.49	0.38	0.62	0.92	0.96	1.28
Al_2O_3	14.84	13.91	14.10	14.12	14.30	7.72	15.77	15.69	15.48	11.07	16.30	14.71	14.26	15.48	15.47	15.59	14.14	14.99	15.54
Fe_2O3_T	1.38	1.24	4.40	2.38	3.30	0.54	2.21	3.31	4.80	0.57	4.21	6.22	5.41	4.70	3.47	8.52	7.63	10.52	12.68
MnO	0.01	0.02	0.04	0.03	0.03	0.01	0.03	0.04	0.07	0.01	0.05	0.08	0.03	0.04	0.04	0.08	0.10	0.10	0.15
MgO	0.35	0.80	1.82	0.95	1.14	0.26	1.03	1.19	1.77	0.22	1.68	2.58	1.45	1.60	1.12	3.46	2.86	2.62	4.98
CaO	0.89	1.83	2.76	1.75	2.06	1.38	3.10	3.57	5.03	2.72	4.04	2.98	3.70	3.04	3.12	1.99	6.32	6.62	7.60
Na_2O	5.57	5.87	5.38	4.27	4.48	2.05	4.83	4.28	3.94	3.17	4.53	3.65	2.42	3.96	4.19	3.66	3.49	3.43	3.31
K_2O	3.12	1.10	2.13	2.92	2.20	0.77	1.28	1.56	0.63	0.40	1.84	2.83	2.48	2.25	2.24	3.13	0.41	0.49	1.98
P_2O_5	0.07	0.01	0.08	0.11	0.14	0.02	0.08	0.10	0.08	0.02	0.14	0.17	0.13	0.10	0.12	0.23	0.15	0.23	0.37
LOI	0.62	0.82	0.78	1.14	1.27	0.67	0.87	0.54	0.96	0.47	2.02	1.16	2.78	1.06	0.43	1.48	0.60	0.80	1.17
Total	99.37	99.99	99.98	99.99	99.96	99.94	99.98	99.94	100.01	99.96	99.95	99.98	99.95	99.94	99.95	99.95	99.99	99.98	99.98
(ppm)																			
Sc	0.75	0.79	5.35	0.86	0.97	0.72	1.40	12.20	11.30	0.40	5.98	15.10	9.45	2.32	9.97	12.50	26.60	26.50	38.60
V	9.94	11.50	79.70	52.90	77.20	10.60	27.20	4.61	60.70	18.00	57.90	171.00	100.0	7.52	14.50	185.00	204.00	221.00	234.00
Cr	1.16	6.66	35.90	7.12	9.90	2.70	11.00	1.97	32.30	2.53	27.70	86.60	61.30	0.50	5.01	118.00	6.63	5.49	51.80
Co	1.67	1.96	8.77	6.46	8.02	2.12	6.60	2.39	11.70	1.49	11.80	18.30	10.30	1.70	3.14	22.30	21.10	21.80	49.50
Ni	0.91	4.06	17.50	6.31	7.45	2.15	10.80	1.74	24.70	4.51	15.60	34.60	21.30	1.36	3.09	38.50	17.60	19.30	59.90
Cu	12.50	6.21	7.66	13.20	15.70	16.00	3.03	2.85	5.92	8.94	4.01	51.20	5.07	1.05	3.85	91.30	38.50	75.50	58.30
Zn	21.90	8.88	17.60	33.90	44.10	8.16	41.40	95.10	46.50	7.08	49.50	68.50	114.0	25.80	68.30	67.70	72.20	71.50	128.00
Ga	16.70	13.10	14.10	15.30	17.20	6.25	18.30	21.60	14.90	8.69	16.60	18.30	18.00	7.36	22.00	17.70	13.80	22.10	22.70
Rb	41.70	37.50	64.80	69.90	62.90	29.70	44.70	75.40	23.40	12.20	66.60	91.90	89.10	41.60	98.50	123.00	5.71	6.78	86.50
Sr	988.00	457.0	458.0	470.0	492.0	121.00	472.00	247.0	180.00	119.00	483.00	499.00	209.0	122.0	394.0	443.00	210.00	233.00	201.00
Y	2.44	1.97	10.80	2.31	2.99	1.62	1.16	45.60	19.40	1.68	5.27	15.80	13.50	6.08	24.80	6.80	18.80	27.00	42.60
Zr	50.70	7.73	172.0	151.0	173.0	374.00	145.00	419.0	123.00	62.90	106.00	163.00	218.0	132.0	422.0	122.00	119.00	102.00	148.00
Nb	2.42	0.68	4.86	3.24	3.75	0.68	5.80	16.30	4.67	0.73	4.09	11.10	9.52	5.82	12.70	11.10	4.50	3.93	13.90
Cs	0.21	0.78	0.80	0.84	0.66	0.39	0.91	1.43	0.79	0.19	2.52	2.13	0.73	0.91	2.05	3.57	0.27	0.43	2.65
Ba	1977.00	258.0	696.0	1185	805.0	138.00	427.00	244.0	163.00	109.00	430.00	1077.0	699.0	111.0	336.0	748.00	49.50	72.20	277.00
La	7.88	8.41	34.60	30.70	55.20	2.73	27.10	30.90	9.60	21.60	14.90	38.50	42.30	8.49	26.60	28.60	5.83	11.20	29.80
Ce	34.30	11.90	56.00	45.00	85.00	3.56	42.70	67.40	21.10	38.40	28.90	69.80	79.40	17.50	56.00	52.10	14.90	29.40	71.50
Pr	1.68	1.01	5.82	3.87	6.74	0.33	3.99	8.81	2.81	3.77	3.42	8.22	9.15	2.05	7.08	5.29	2.26	4.37	9.29
Nd	6.03	3.30	18.90	11.00	18.90	1.16	12.60	37.90	12.70	13.40	13.70	30.30	34.90	8.32	28.90	18.80	11.30	21.60	40.40
Sm	0.91	0.53	2.51	1.17	1.76	0.14	1.19	8.30	3.07	1.80	2.20	4.86	5.65	1.59	5.87	2.57	2.76	4.98	8.32
Eu	0.60	0.82	0.92	0.52	0.69	0.17	0.36	2.32	0.82	0.38	0.62	1.07	1.11	0.48	1.88	0.83	0.86	1.26	1.67
Gd	0.76	0.49	2.48	1.20	1.92	0.18	0.89	7.57	3.19	1.45	1.66	4.27	4.91	1.31	4.93	2.17	3.02	4.80	7.84
Tb	0.10	0.07	0.38	0.12	0.18	0.03	0.07	1.55	0.65	0.12	0.23	0.61	0.66	0.23	0.89	0.28	0.54	0.91	1.36
Dy	0.47	0.31	1.79	0.49	0.69	0.14	0.34	8.50	3.59	0.45	0.93	3.05	3.09	1.11	4.56	1.34	3.51	5.33	7.72
Ho	0.09	0.06	0.36	0.08	0.09	0.05	0.04	1.75	0.72	0.07	0.15	0.54	0.49	0.23	0.96	0.23	0.74	0.99	1.50
Er	0.27	0.18	1.03	0.23	0.29	0.22	0.13	5.06	2.27	0.20	0.54	1.58	1.27	0.61	2.77	0.67	2.15	2.95	4.74
Tm	0.05	0.02	0.18	0.03	0.03	0.05	0.02	0.82	0.34	0.03	0.07	0.25	0.18	0.10	0.44	0.11	0.31	0.41	0.72
Yb	0.28	0.17	1.29	0.17	0.20	0.46	0.13	5.21	2.36	0.25	0.51	1.53	1.03	0.67	3.35	0.72	2.19	2.73	4.86
Lu	0.04	0.03	0.20	0.03	0.04	0.12	0.02	0.79	0.38	0.05	0.08	0.22	0.15	0.10	0.53	0.11	0.33	0.46	0.75
Hf	1.55	0.19	4.56	4.13	4.62	12.50	4.19	10.80	4.15	2.78	3.25	5.00	6.44	3.68	11.00	3.66	3.33	2.99	4.55
Ta	0.06	0.06	0.38	0.16	0.22	0.32	0.38	1.09	0.72	0.50	0.57	0.62	0.61	0.22	0.67	0.69	0.40	0.34	1.29
Pb	15.80	9.87	11.30	16.80	20.10	2.07	6.57	11.50	2.48	2.27	8.99	21.10	24.70	4.69	14.40	13.40	2.13	2.48	8.08
Th	2.82	0.76	6.57	12.60	29.70	0.31	5.08	4.26	1.24	4.66	4.36	7.55	12.20	1.35	3.78	7.58	0.18	0.46	3.07
U	0.40	0.55	0.53	0.38	0.49	3.85	0.30	0.86	0.45	2.19	3.55	0.50	1.54	0.27	0.68	0.75	0.20	0.27	1.07

Notes: LOI = loss on ignition.

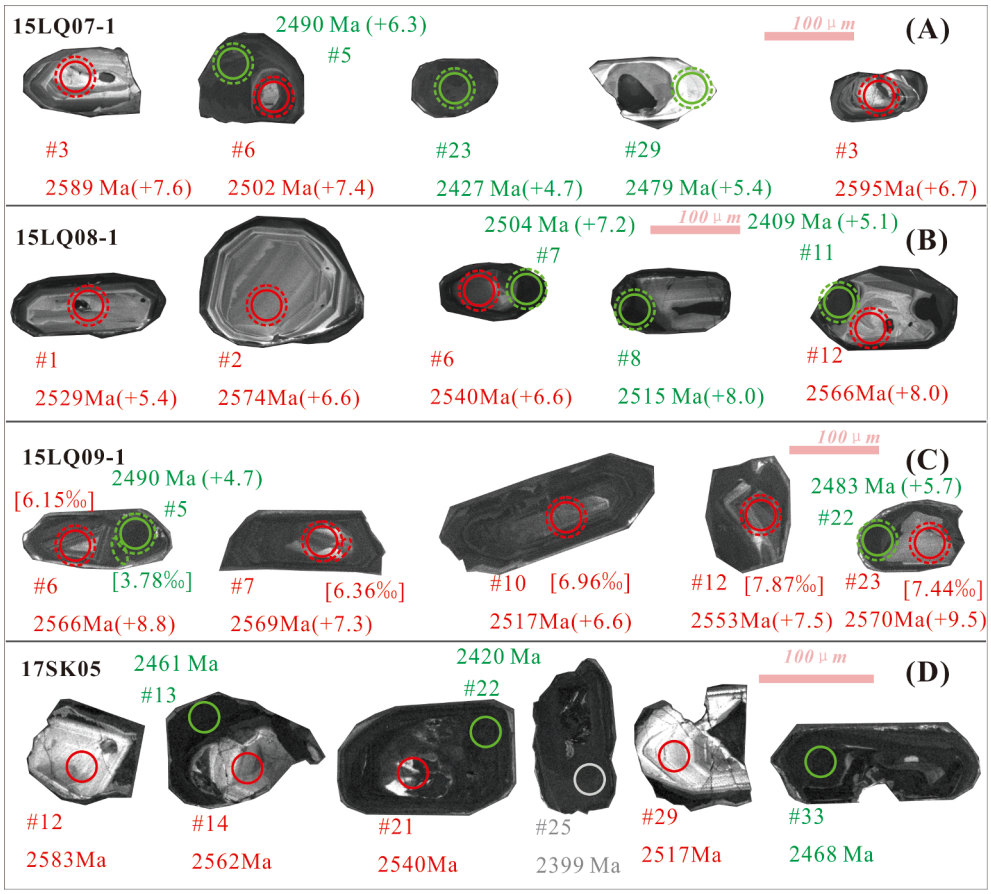

Fig. 3. CL images for representative zircons from the granitoid gneisses in northern Liaoning. The red, green and grey solid circles represent U–Pb dating sites of the magmatic, metamorphic and later-thermal-event domains of zircons, respectively. The red and green dashed circles represent Hf isotope sites of the magmatic and metamorphic domains of zircons, respectively. The red and green dashed ellipses represent O isotope sites of the magmatic and metamorphic domains of zircons, respectively. The numbers near the circle are the spot number, U–Pb age, $\varepsilon_{Hf}(t)$ value in round bracket and the $\delta^{18}O$ value in the in square bracket. (For interpretation of the references to color in this figure legend, the reader is referred to the web version of this article.)

0.05 on average). The rim analyses define an upper intercept age of 2491 ± 18 Ma (MSWD = 0.3, n = 9) and give a weighted mean $^{207}Pb/^{206}Pb$ age of 2495 ± 7 Ma (2483–2512 Ma; MSWD = 1.0, n = 9; Fig. 4C).

Fifty analyses were obtained from sample 17SK05. The magmatic zircon cores have Th of 136–286 ppm (136 ppm on average) and U of 99–359 ppm, (229 ppm on average), yielding slightly high Th/U ratios (0.40–0.84, 0.60 on average). The core analyses define an upper intercept age of 2499 ± 57 Ma (MSWD = 3.4, n = 11), which is consistent with the weighted mean $^{207}Pb/^{206}Pb$ age of 2506 ± 9 Ma (2461–2583 Ma; MSWD = 5.0, n = 14; Fig. 4D). The metamorphic rims contain Th of 2–454 ppm (143 ppm on average) and U of 132–3546 ppm (1560 ppm on average), yielding much lower average Th/U ratio of 0.13 than that of the magmatic cores. The rim analyses define an upper intercept age of 2453 ± 18 Ma (MSWD = 1.3, n = 29) and yield a weighted mean $^{207}Pb/^{206}Pb$ age of 2459 ± 5 Ma (2405–2522 Ma; MSWD = 5.1, n = 29; Fig. 4D). The later-thermal-event zircon group contains nine analyses and define an upper intercept age of 2404 ± 69 Ma (MSWD = 5.3)

In summary, the $^{207}Pb/^{206}Pb$ age of the magmatic cores (2519 ± 13, 2556 ± 4, 2542 ± 5 and 2506 ± 9 Ma) reflect the crystallization ages of the magmatic precursors for the granitoid gneisses in northern Liaoning, whereas the metamorphic rims represent a subsequent regional metamorphic event at 2496–2456 Ma. Then the ancient zircons have been affected by a later thermal event (Fig. 4; Table 1).

4.2. Zircon Hf isotope

The dated spots from the granitoid gneisses in northern Liaoning (15LQ07-1, 15LQ08-1 and 15LQ09-1) were analyzed for Lu–Hf isotopes (Table 2). The dioritic gneiss shows nearly consistent $^{176}Hf/^{177}Hf$ ratios (0.281343–0.281412 for the magmatic cores and 0.281362–0.281414 for the metamorphic rims). As with the tonalitic gneiss, the $^{176}Hf/^{177}Hf$ ratios of the magmatic core analyses show a relatively wide range (0.281331–0.281520), yet similar to those of the metamorphic rim (0.281378–0.281534). This indicates a generally undisturbed Lu–Hf isotope system, though some zircons have undergone Pb loss (Fig. 5 a, b; Supplemental File 3; Griffin et al., 2000; Tang et al., 2014). In contrast, the magmatic core analyses of the trondhjemitic gneiss have higher $^{176}Hf/^{177}Hf$ ratios (0.281425–0.281530, 0.281468 on average) than those of the metamorphic rims (0.281366–0.281469, 0.281403 on average), indicating an open-system behavior for the Lu–Hf isotope. The analyses show consistently high $\varepsilon_{Hf}(t)$ values between the chondrite and the depleted mantle evolution lines: (i) dioritic gneiss yields $\varepsilon_{Hf}(t)$ value of +3.6 to +9.2, with T_{DM} of 2.52–2.70 Ga and T_{DM2} of 2.57–2.88 Ga; (ii) tonalitic gneiss has $\varepsilon_{Hf}(t)$ value of +3.0 to +9.0, with T_{DM} of 2.53–2.66 Ga and T_{DM2} of 2.46–2.90 Ga; and (iii) trondhjemitic gneiss shows $\varepsilon_{Hf}(t)$ value of +4.5 to +9.5, with T_{DM1} of 2.51–2.66 Ga and T_{DM2} of 2.43–2.83 Ga.

4.3. O and Nd isotope

The $\delta^{18}O$ values of the magmatic zircon cores from the trondhjemitic gneiss range from 6.0‰ to 7.9‰, with an average of 6.9‰, whereas the lower $\delta^{18}O$ values of the metamorphic rims range from 3.8‰ to 5.2‰, with an average of 5.2‰. The distinguished $\delta^{18}O$ values between the magmatic zircon cores and metamorphic rims within sample 15LQ09-1 reveals an open system for the oxygen isotope during metamorphism and high-temperature water–rock interaction (Valley et al., 2003, 2005). The fractionation of the oxygen isotopes varies with mineralogy and exhibit a linear relationship of wt % SiO_2 for igneous rocks at magmatic temperatures. That is, the liner fit yields the equation: $\delta^{18}O$ (zircon) – $\delta^{18}O$(whole rock) ≈ –0.0612 × (wt.% SiO_2) + 2.5‰ (Valley

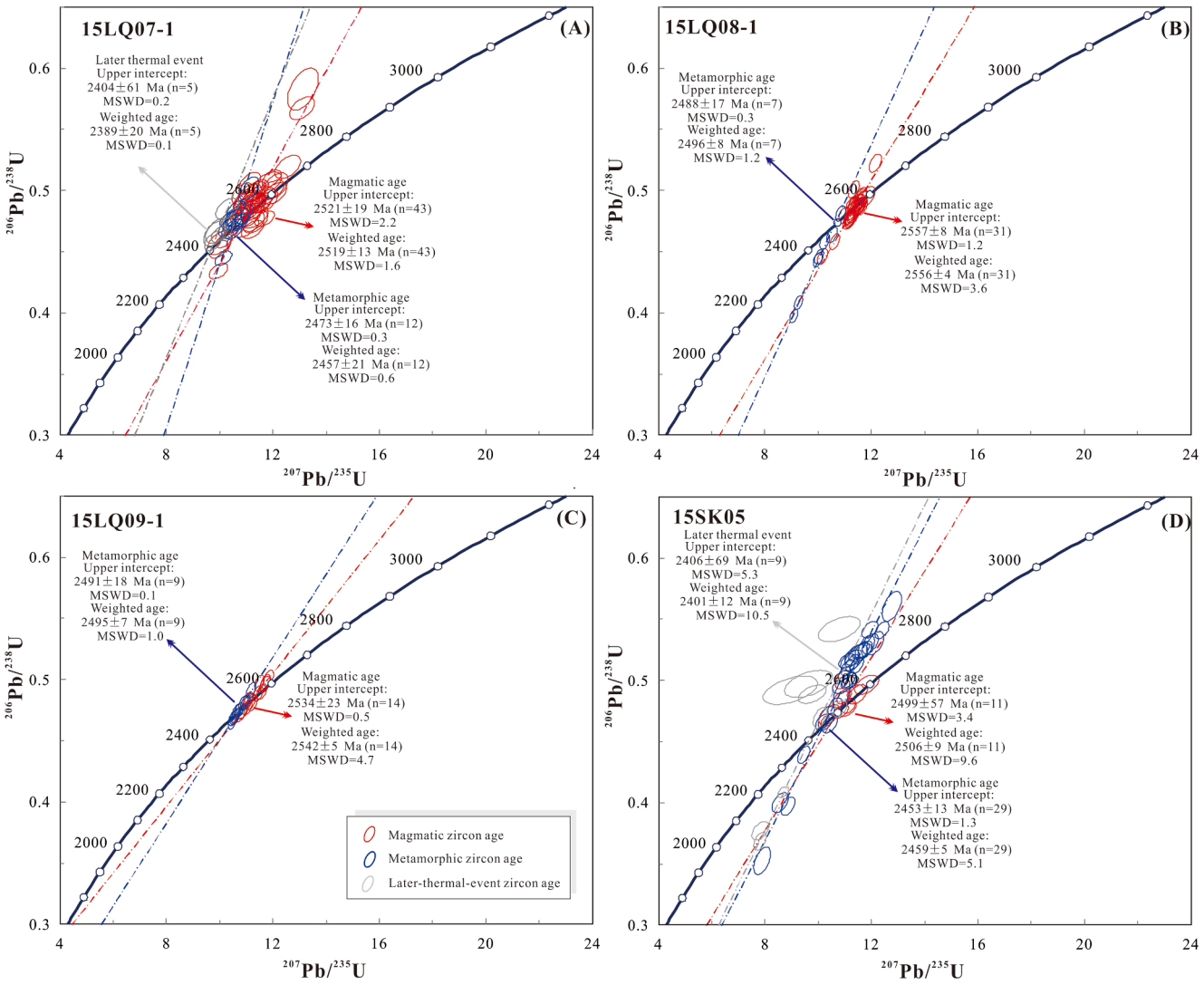

Fig. 4. U–Pb zircon concordia diagrams for the granitoid gneisses in northern Liaoning.

et al., 1994; Lackey, 2005). The calculated $\delta^{18}O$ value of the zircons within the trondhjemitic gneiss is 5.6‰ and is consistent with the obtained zircon $\delta^{18}O$ values, which exhibit equilibrium O isotope fractionations between whole rock and zircon. The calculated $\delta^{18}O$ values of the zircons within the tonalitic and dioritic gneisses are 6.0‰ to 8.3‰ (7.1‰ on average), and 6.4‰ to 10.3‰ (7.8‰ on average), respectively. The dioritic and TTG gneisses have ε_{Nd}(2.5 Ga) values of + 3.3 to + 5.1 and + 0.8 to + 5.4, respectively, with variable initial Nd isotopic ratios (Table 3).

4.4. Major and trace elements

The granitoid gneisses in northern Liaoning are subalkaline with low concentrations of alkali metals ($Na_2O + K_2O$ = 2.8–8.7 wt%; Table 4), plot across the boundary between metaluminous and peraluminous fields, and belong to medium-K calc-alkaline to low-K tholeiitic suites of high Na_2O/K_2O ratios (>1, some even > 4) (Supplemental File 4). The dioritic gneisses contain low SiO_2 concentrations (50.91–63.37 wt%) and thus belong to gabbro and diorite, whereas the TTG gneisses have higher SiO_2 concentrations (64.72–86.46 wt%) and plot in the granite and granodiorite fields in the TAS diagram (Irvine and Baragar, 1971; Middlemost, 1994), consistent with observation in the Ab–An–Or diagram (Supplemental File 4). They are enriched in light REEs (LREEs), with the dioritic and TTG gneisses having $(La/Yb)_N$ (N means chondrite-normalized) ratios of 1.8–26.7 (8.8 on average) and 6.0–281.5 (68.1 on average), respectively. The granitoid gneisses both show weakly negative to positive Eu anomalies in the chondrite-normalized REE patterns and negative Ti anomalies in primitive mantle-normalized spider diagrams (Sun and McDonough, 1989). They are enriched in the large ion lithophile elements (LILEs; e.g., Rb, Sr, and Ba) but depleted in the high field strength elements (HFSEs; e.g., Nb, Ta, Zr, and Hf; Supplemental File 5).

5. Discussion

5.1. Petrogenesis of the Neoarchean granitoid gneisses in northern Liaoning

Integrated our newly obtained data with reliable studies on the geochronology, the early Precambrian geological event series in northern Liaoning can be summarized as below. Compared with the eastern Liaoning where the Eoarchean rocks are exposed (Liu et al., 2008; Song et al., 1996; Wan et al., 2005c, 2012), the oldest basement in northern Liaoning are Mesoarchean granodioritic–tonalitic gneisses at Luanjiajie (3.0 Ga; Li et al., 2020; Liu et al., 2017). The 2.68 Ga amphibole plagioclase gneiss is the only early Neoarchean lithotectonic record in northern Liaoning (Wang et al., 2016a), whereas the correct ages still need more detailed study to be proved (Li and Chen, 2019). According to

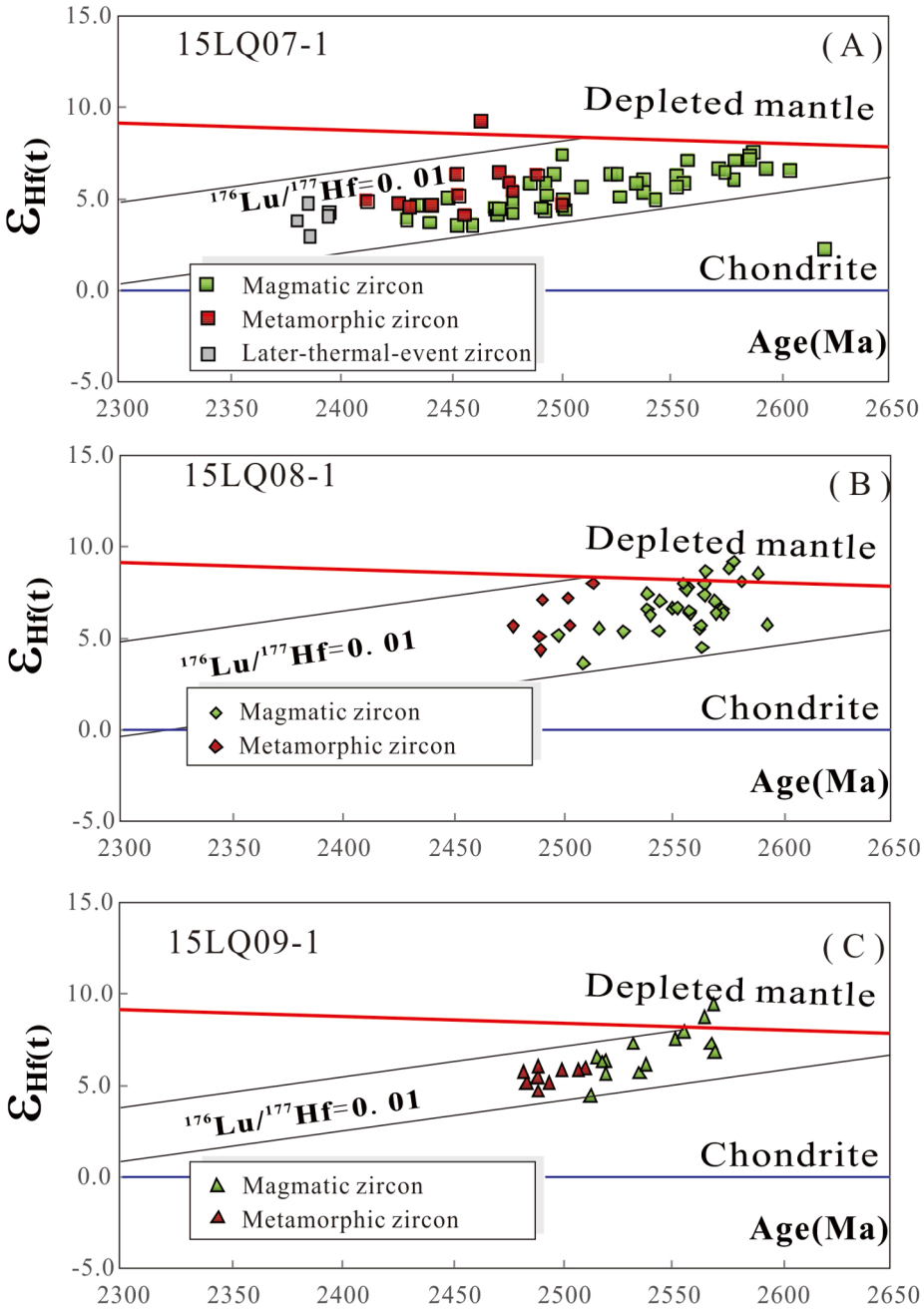

Fig. 5. Zircon $\varepsilon_{Hf}(t)$ versus t (Ma) diagram for the granitoid gneisses in northern Liaoning.

the agreement of the intrusive timing within error permissibility (dioritic gneiss: 2519 ± 13, tonalitic gneiss: 2556 ± 4, trondhjemitic gneiss: 2542 ± 5 and 2506 ± 9 Ma; Fig. 4) and closely spatial relationship (Fig. 2), we suggest a synchronism for the above rock units. These late Neoarchean lithotectonic assemblages are coeval with the volcanism and sedimentation within the Qingyuan greenstone belt (Li and Wei, 2017; Peng et al., 2015; Wang et al., 2016a, 2016b; Wu et al., 2016). Temporally overlapping but slightly younger timing than the magmatism event is the regional metamorphism event recorded by the metamorphic zircon rims with ages of 2496–2456 Ma (Fig. 4). The nearly coeval magmatism and metamorphism constitute the most significant tectono-thermal event in northern Liaoning, which also characterizes the late Neoarchean evolution of the Eastern Block (Zhao and Zhai, 2013; Zhao et al., 1998, 2001, 2005). The magmatic precursors of the granitoid gneisses in northern Liaoning are formed coevally at the end of the Neoarchean, despite their different isotopic and geochemical compositions. That is to say, individual types were not derived from the same magma source or generated by the same magmatic process.

5.1.1. Dioritic gneisses: quenched inclusions rather than lithospheric relics

The xenoliths in the Archean granitoid gneisses within the Eastern Block, North China Craton, include peridotite, amphibole pyroxenite and amphibolite, ect (Li et al., 2019c; Liu and Zhang, 2019; Peng et al., 2015; Yang and Wei, 2017a, 2017b; Wang et al., 2020), which represent either fragments of the lithospheric mantle or cumulates/crystallizations from ultramafic magma at individual mantle depths (Bodinier and Godard, 2014; Griffin et al., 1999; Lee et al., 2001; Wang et al., 2019; Whattam and Stern, 2011). For example, the ultramafic xenolith (serpentinite) distributing as dyke-like bodies in the quartz diorite and TTG from Pinglinghou, northern Liaoning, were highly serpentinized, with varied amounts of orthopyroxene and minor spinel (Peng et al., 2015). In eastern Hebei, the mafic granulites as xenoliths were recognized

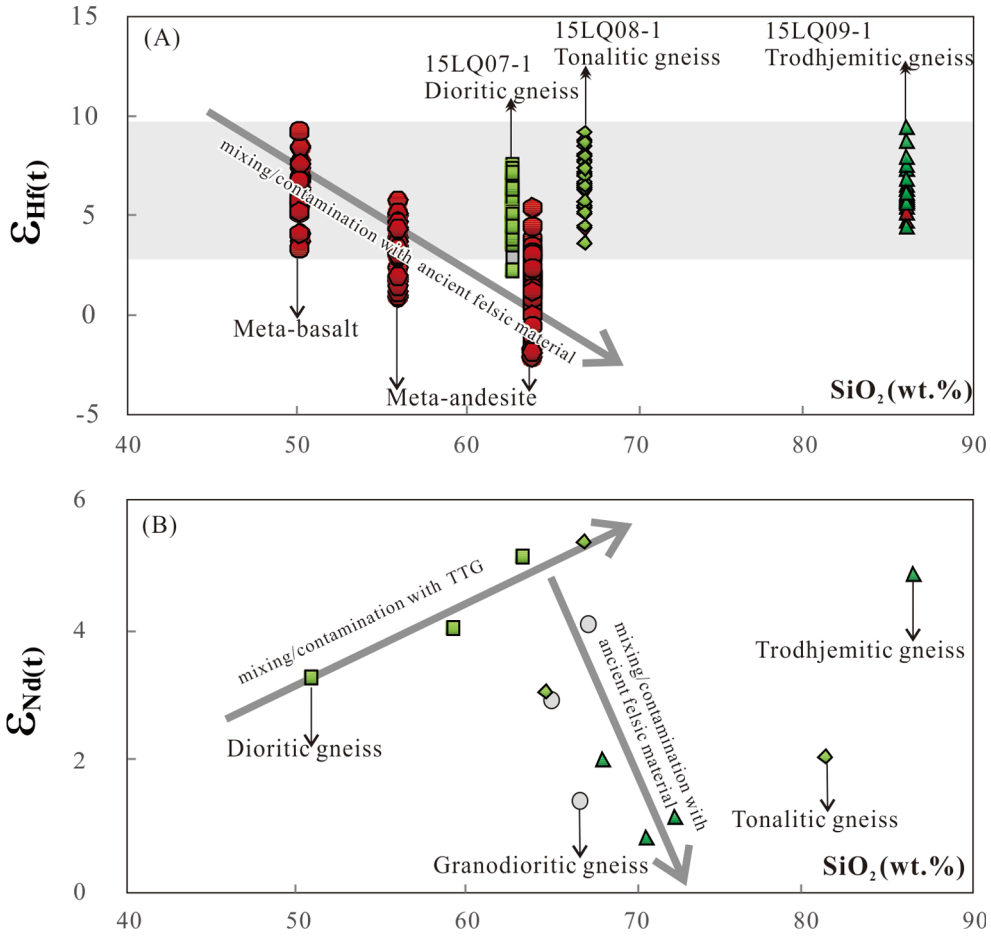

Fig. 6. (A) Zircon $\varepsilon_{Hf}(t)$ versus SiO_2 and (B) $\varepsilon_{Nd}(t)$ versus SiO_2 diagrams for the granitoid gneisses in northern Liaoning.

involving the garnet -bearing or garnet-free two-pyroxene granulites from Taipingzhai and Saheqiao, and garnet clinopyroxene or pyroxenite granulites from the Malanyu (Yang and Wei, 2017a, 2017b), whereas those are spinel lherzolites in Songling and Majiayu (Gong and Li, under review). The former have a mineral assemblage of mostly clinopyroxene, plagioclase, amphibole, and minor quartz, ilmenite and apatite, with or without garnet, orthopyroxene and biotite (Yang and Wei, 2017a), in contrast to the latter containing olivine (45%–59%) + orthopyroxene (25%–34%) + clinopyroxene (9–16%) + amphibole (3–5%) + minor spinel (1–5%). Notably, the above xenoliths show different mineral compositions and textures from the dioritic gneisses with an assemblage of plagioclase, amphibole, and minor quartz (detailed description of mineral assemblage refers to the "Geological background" section) in spite of their similar color in outcrop and generally weakly gneissic to massive structures (Fig. 2). Thus, the dioritic gneisses in northern Liaoning are inconsistent with the xenoliths, rather suggest the occurrences as mafic microgranular enclaves (MMEs) within the host TTG gneisses.

After excluding the possibility of the xenolith, the MMEs can yet be generated via (i) early crystallization from the basaltic magma (Noyes et al., 1983), (ii) incorporation of the residual phases from the magma source (White et al., 1999) or the country rocks during the emplacement, or (iii) mixing between externally injected mafic and the host felsic magma (Chen et al., 2009; Sklyarov and Fedorovsky, 2006), we plumped for mixing model as the best candidate for the MMEs within the host Neoarchean TTG gneisses in northern Liaoning for the following lines of evidence. (i) The original magmatic precursors of MMEs are micro- to fine-grained diorites, inferred from their fine-grained textures even after metamorphism (Fig. 2 B–F, I). This preclude the possibility of mineral cumulates from mafic magma, which otherwise are characterized by the coarse-grained and cumulative textures via early crystallization (Noyes et al., 1983). This is verified by the high Sc (12.5–38.6 ppm) and Co (21.1–49.5 ppm) abundances of the MMEs. (ii) The coeval nature of the MMEs and host rocks was supported by the similar zircon U–Pb ages of the two rock units present in this contribution. Thus, models for the MMEs as refractory and residual phases after partial melting can be also rejected, which otherwise have partial melted veinlets from source-rock anatexis and thus relatively low SiO_2 and high MgO contents (e.g., Chappell and White, 1992). (iii) MMEs occur as rounded to ellipsoidal globules, and are sometimes highly elongated within the host, likely as a result of magma mixing between an externally injected mafic magma and host felsic magma, that is quenched inclusions (Chen et al., 2009; Sklyarov and Fedorovsky, 2006). The globules in shape and no solid-state deformation may indicate stretching plastically within a partially crystallized (Fig. 2B, C). The *syn*-plutonic mafic dykes observed within the TTG gneisses in northern Liaoning (Fig. 2D–F) also suggest a hybrid origin, as also recognized in southern Jilin and South Africa, etc (Li et al., 2019c). Thus, mafic magma as dykes injected in the felsic magma chamber, and then *syn*-plutonic mafic dykes broke up into discrete globules to form the MMEs. In addition, the hybrid origin of the MMEs is supported by the large variations in whole-rock chemistry and isotope, which argue for a heterogeneous mixing (Figs. 7 and 8; Supplementary File 4 and 5). The lower SiO_2 and higher MgO contents than crustal melts suggest that the precursor of the MME could be a basaltic magma (Eiler et al., 2000; Gill, 1981; Grove and Donnelly-Nolan, 1986; Grove et al., 2003).

Additionally, the dioritic gneisses also underwent significant fractional crystallization of ferromagnesian phases (Table 4), as evidenced

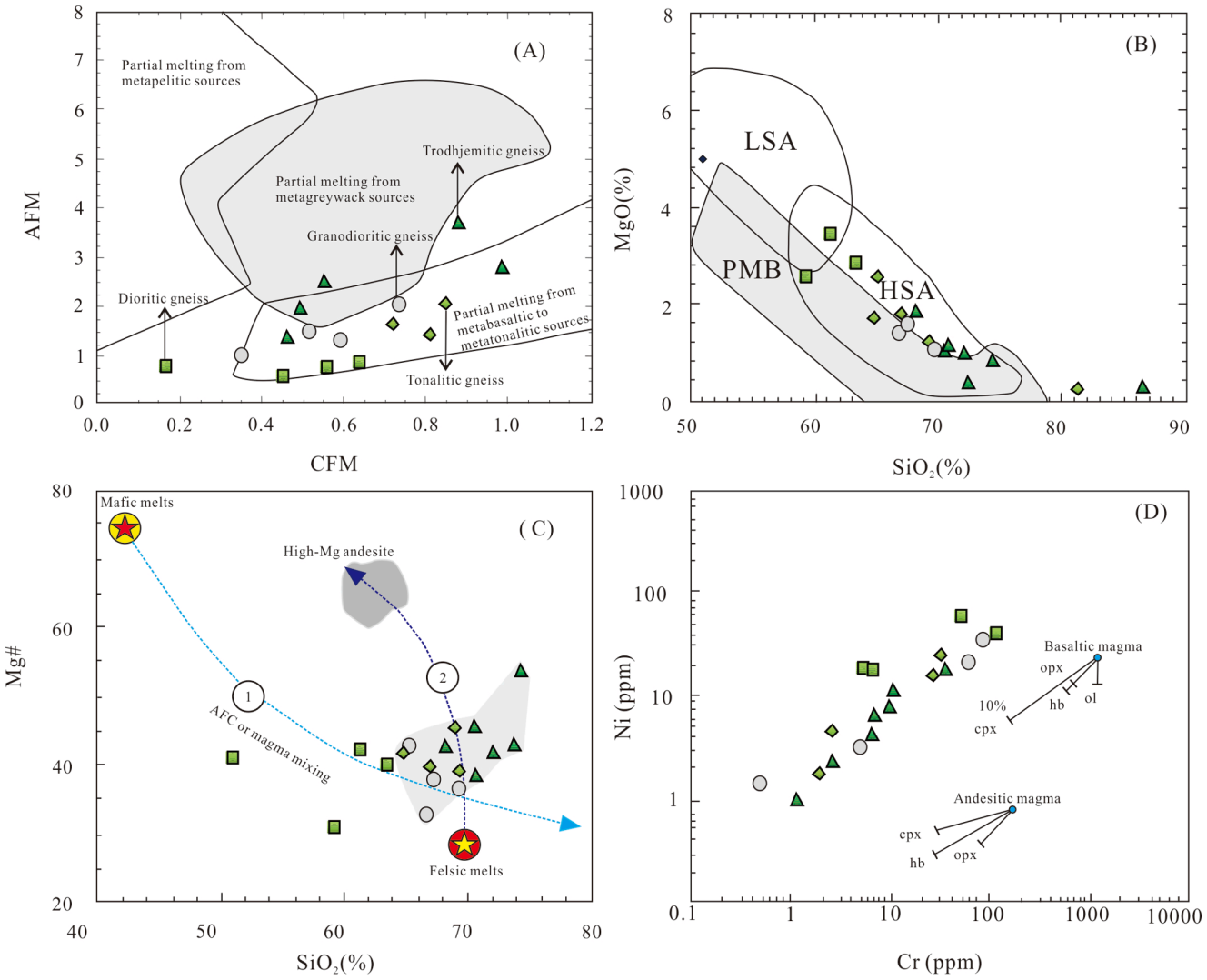

Fig. 7. (A) AFM versus CFM diagram, showing potential sources of the granitoid gneisses in northern Liaoning (modified from Altherr et al. (2000)). (B) MgO versus SiO_2 diagram. PMB, experimental partial melts from basalts or amphibolites; LSA, low-silica adakite; HSA, high-silica adakite; (modified after Martin et al., 2005). (C) Mg-number versus SiO_2 diagram. The fields of mantle-derived mafic melt and felsic melts from partial melting of garnet amphibolite and eclogite are from Kelemen (1995), Stern and Kilian (1996) and Rapp et al. (1999). (D) Ni versus Cr diagram. The partition coefficients are from Rollision (1993). Ol, olivine; Opx, orthopyroxene; Cpx, clinopyroxene; Hb, hornblende.

by the primary mantle-derived melts with high contents of Ni and Cr (>400 and >1000 ppm, respectively; Wilson, 1989). The ε_{Hf}(2.5 Ga) of the dioritic gneisses vary over a large range (+3.5 to +9.0), which confirm an open system for the magma system (Fig. 5A). The ascent of enclave-forming magma injecting into the host was often associated with crustal contamination. The lower ε_{Hf}(2.5 Ga) and ε_{Nd}(2.5 Ga) values of the dioritic gneisses than those of the coeval basaltic–andesitic magma are indicative of weak contamination by ancient felsic crusts (e.g., 3.0 Ga granodioritic gneisses in the vicinity, Li et al., 2020) or mixing with siliceous crustal melts that have unradiogenic ε_{Nd}(2.5 Ga) and ε_{Hf}(2.5 Ga) compositions (Fig. 6). Furthermore, the calculated zircon $\delta^{18}O$ values (6.4‰–6.6‰) are higher than those of mantle-derived magma (Eiler et al., 2000; Valley et al., 2003, 2005; Zhang et al., 2012a, 2012b), also revealing an addition of supracrustal component into the magma source. The process of mixing with the felsic host magma did occur, notwithstanding it was based on neither chemical transfer nor transfer of crystals between MMEs and host rocks due to subsequent deformation and metamorphism. The process can be revealed by the positive correlation between the ε_{Nd}(2.5 Ga) values and SiO_2 contents (Fig. 6B), as the tonalitic gneiss (15LQ08-1) with both high ε_{Nd}(2.5 Ga) value and SiO_2 content would be the best candidate. Therefore, a possible genetic model is that the *syn*-plutonic dykes and MMEs originated from a mantle source, then evolved via fractional crystallization and contamination/mixing with ancient felsic materials, and finally were injected into the host TTG magma and experienced mixing with the latter. The mantle sources provided both heat and materials to form the host TTG gneisses, indicating the crustal growth at *ca.* 2.5 Ga.

5.1.2. *TTG gneisses: Partial melting of juvenile basaltic sources*

The evidence for partial melting of juvenile basaltic sources as the predominant derivation of the TTG *gneisses* in northern Liaoning includes: (i) in the AFM (molar Al_2O_3/(MgO + total FeO)) versus CFM (molar CaO/(MgO + total FeO)) diagram (Fig. 7A; Altherr et al., 2000), TTG gneisses mainly display low CFM but high AFM values, plotting in the field of partial melting from basaltic to tonalitic rocks; (ii) they share similar characteristics with experimental partial melts from meta-basalts in the MgO versus SiO_2 diagram (Fig. 7B; Martin et al., 2005); and (iii) the zircon ε_{Hf}(2.5 Ga) values of the tonalitic and trondhjemitic gneisses (15LQ08-1 and 15LQ09-1) are consistent with those of the coeval meta-basalts, but higher than those of the meta-andesites (Fig. 6A). Conspicuously, some TTG gneisses with higher MgO

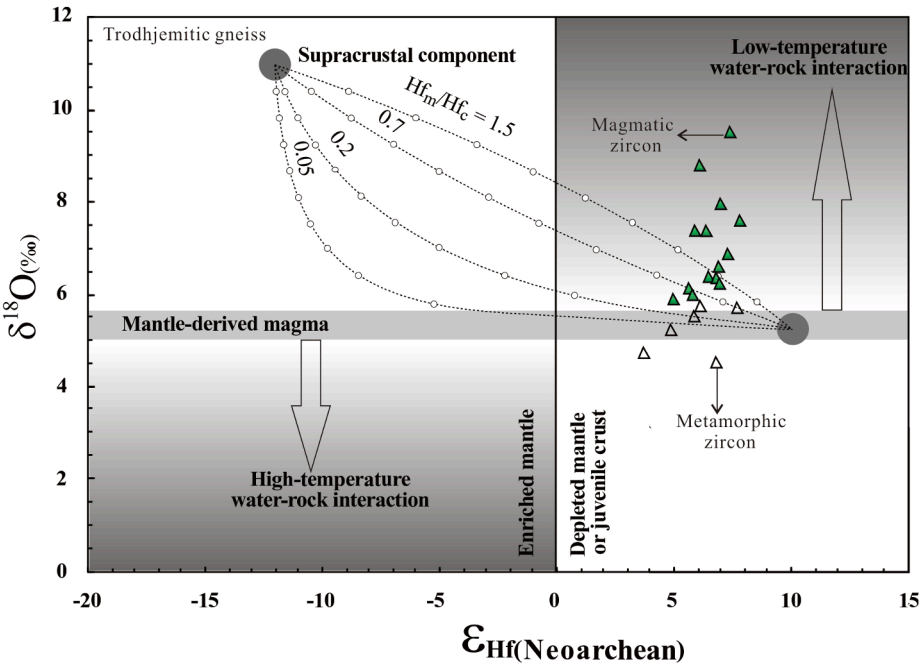

Fig. 8. Plot of zircon Hf versus O isotope. All $\varepsilon_{Hf}(t)$ were calculated with the t = 2.5 Ga. The dotted line denotes the mixing trend between the mantle- and supercrust-derived components. Hf_m/Hf_c in the curve is the ratio of Hf concentration in the mantle (m) over crustal (c) component, and the small open circle on the curve represents 10% mixing increment by assuming that the mantle magma has $\varepsilon_{Hf}(t) = 17$ and $\delta^{18}O = 5.3‰$ and the supracrustal zircon $\varepsilon_{Hf}(t) = -7$ and $\delta^{18}O = 10‰$ (modified after Zhang et al., 2012a, Zhang et al., 2012b).

contents plot in the HSA field, which seems to indicate that the sources to produce the high-Mg melts would be necessary (Fig. 7B). In the Mg# versus SiO_2 diagram (Fig. 7C), the TTG gneisses show a trend defining a process of felsic melt-peridotite interaction (Rapp and Watson, 1995; Rapp et al., 1999), also supporting an addition of high-Mg melts in the magma process. The most likely mechanism to produce the high-Mg melts is to evolve from Archean komatiitic magma (Li et al., 2019b; Peng et al., 2015; Zhai et al., 1985), which obviously needs more detailed petrological and geochemical study to be constrained. Partial melting of juvenile basaltic sources occurs due to thermal input from the rising high-Mg melts with anomalously high temperatures (Li and Wei, 2017).

The relatively wide ranges of ε_{Hf}(2.5 Ga) and ε_{Nd}(2.5 Ga) values support magma mixing or contamination process, rather than derivation from a relatively homogeneous pristine source (Fig. 6A, B). The ε_{Hf}(2.5 Ga) values of the tonalitic and trondhjemitic gneisses remained unchanged along with SiO_2 contents increasing, while the ε_{Nd}(2.5 Ga) values negatively correlate with SiO_2 contents (Fig. 6A, B). The "pseudo decoupling" of Hf and Nd isotopes may attribute to different closure temperatures, that is during the magma process, zircon Hf system records early fractional crystallization (Fig. 7D) and mixing with the basaltic magma for its relatively high closure temperature, whereas the whole-rock Nd isotope reveals contamination of an ancient felsic crust at the late stage. Some TTG gneisses plotting in the meta-greywacke field indicate contamination of felsic crustal material indeed (Fig. 7A). In sum, the rising high-Mg melts provided both heat to trigger parting melting of juvenile basaltic sources and materials to form the parental TTG magma, then the parental TTG magma evolved via fractional crystallization and mixing with MMEs, and finally experienced crustal contamination of the sedimentary rocks. The high ε_{Hf}(2.5 Ga) and ε_{Nd}(2.5 Ga) values between the depleted mantle and chondrite, together with the young T_{DM} (mainly 2.8–2.5 Ga), suggest an origin of the depleted mantle indirectly, which is also consistent with the large variations in Neoarchean zircon $\delta^{18}O$ values. On the $\delta^{18}O$ versus ε_{Hf}(2.5 Ga) diagram (Fig. 8; Zhang et al., 2014), the most concordant zircons plot across the mixing line between 3.5 Ga continental crust (assuming $\delta^{18}O = 10‰$) and the depleted mantle with a Hf concentration ratio (Hf_m/Hf_c) of 1.5. According to the zircon Hf–O isotopic modeling, about 80% of the parent magma of the Neoarchean granitoids rocks are formed by partial melting of the lower juvenile basaltic crust (which, in turn, originated from a depleted mantle source), implying that the TTG gneisses in northern Liaoning is a signal of Neoarchean crustal growth.

5.2. *Implications for the adakitic signature*

As mentioned above, an issue of major dispute in the petrogenesis of TTG worldwide has long existed over its adakitic signature (Martin, 1986; Moyen, 2009, 2011; Moyen and Stevens, 2006). The common belief for the TTG is derivation from the garnet amphibolite or eclogite (e.g., Bédard, 2006; Beard and Lofgren, 1991; Condie, 1986, 1998; Foley et al., 2002; Martin, 1986, 1994, 1999; Moyen, 2011; Moyen and Stevens, 2006; Xiong et al., 2005). The partial melting of the hydrous basalts in the garnet stability field would elevate the TTG magma with high Sr/Y and La/Yb ratios, an analogue of Cenozoic adakite (Kay, 1978; Defant and Drummond, 1990; Yang et al., 2008), as Sr and La partition coefficients for garnet are much lower than the remaining two (Klein et al., 1997; Ronov and Yaroshevsky, 1976; Rollision, 1993; Smithies, 2000). Since the discovery of adakite in some modern arcs (Defant and Drummond, 1990), extensive literatures have recognized it as a suit of intermediate to felsic volcanic or intrusive rocks with salient geochemical and isotopic features (such as high Sr/Y (≥40) and $(La/Yb)_N$ (≥20)), originally interpreted as a derivation by partial melting of the young and hot subducted slab (e.g., Martin, 1999; Moyen, 2009, 2011). Over time, geochemistry (e.g., elevated Sr/Y) of the adakite and TTG with adakitic signature were gradually used to constrain the depth of melting (Castillo, 2012; Moyen, 2009). However, in this contribution we tentatively highlight other new factors to produce such magma. (i) The TTG magma is derived from the partial melting of the meta-basalts, whereas the geochemical traits of the basalts are not well constrained. At least two kinds of Archean basalts were recognized (Condie, 1981; Li and Wei, 2017), viz. TH1-type basalt enriched in LREEs and LILEs, and depleted in HFSEs and HREEs, similar to the arc basalt; and TH2-type basalt characterized by LREE-depleted to slight LREE-enriched chondrite normalized REE patterns and near-flat primitive mantle normalized patterns, which are similar to those of normal mid-ocean ridge basalt (Ordóñez-Calderón et al., 2009; Sun and McDonough, 1989) or ocean-plateau tholeiites (Mahoney et al., 1993; Révillon et al., 2000; Xie et al., 1993). Take $(La/Yb)_N$ versus $(La)_N$ as an example, we recalculated

the values based on different La and Yb contents. If TTG magma is the product of the TH1-type basalt, the garnet in source is needed much less than that of TH2-type basalt. (ii) Fractional crystallization of amphibole or clinopyroxene also contributes to the high Sr/Y and La/Yb ratios due to large Y and Yb partition coefficients for two minerals (Klein et al., 1997). (iii) TTG may experience crustal contamination prior to emplacement. The crustal contamination, such as greywacke, commonly show the enrichment of LREEs and LILEs, and depletion of HFSEs and HREEs (Rollision, 1993), which might also elevate the Sr/Y and La/Yb ratios. (iv) MMEs within the host TTG evolve from the basaltic magma via fractional crystallization and experience crustal contamination both resulting in the elevated Sr/Y and La/Yb ratios of the whole rock as aforementioned. Therefore, we propose that mineralogical composition or to say the pressure conditions of the crustal anataxis is not the only cause of adakitic features of TTG and other factors also play an important role, which was used to be overlooked worldwide.

6. Conclusions

The salient conclusions arising from our synthesis are as follows:

(1) The precursors of the Neoarchean granitoid gneisses, viz. TTG and dioritic gneisses, in northern Liaoning were contemporaneously emplaced between 2.56 and 2.51 Ga, reflecting a giant Neoarchean igneous event throughout eastern North China Craton. Subsequently they were subjected to regional amphibolite- to granulite-facies metamorphism at 2.48–2.45 Ga.

(2) TTG gneisses, as partial melts from juvenile basaltic sources, evolved via mixing with mafic enclaves and fractional crystallization, and finally were assimilated by the continental sedimentary rocks.

(3) Both TTG and dioritic gneisses are products of Archean crustal growth, though the magmatic processes are not exactly the same.

(4) The adakitic signature of the TTG may be affected by nature of the sources, magma mixing, fractional crystallization, and crustal contamination, rather than solely controlled by the pressure conditions of crustal anataxis.

CRediT authorship contribution statement

Zhuang Li: Conceptualization, Methodology, Writing - original draft. **Chunjing Wei:** Resources, Supervision, Funding acquisition, Writing - review & editing. **Bin Chen:** Supervision, Funding acquisition. **Wei Zhang:** Data curation, Investigation. **Fan Yang:** Data curation, Investigation.

Declaration of Competing Interest

The authors declare that they have no known competing financial interests or personal relationships that could have appeared to influence the work reported in this paper.

Acknowledgements

The final version of the paper benefited from the constructive comments and careful corrections of the Journal Editor Prof. Guochun Zhao and two anonymous journal reviewers. We are grateful to Dr. Yan Zhan of *University of Illinois at Urbana-Champaign* and Dr. Mingyue Gong of *Peking University* for their perceptive suggestions and careful corrections on preparing the manuscript for this paper. Helps from Dr. Bin Fu of *Australian National University* and Dr. Wei Tian of *Peking University* are appreciated. Our work was supported financially by the Science Foundation of China University of Petroleum, Beijing (Grant Number: 2462017YJRC032) and the National Natural Science Foundation of China (Grant Numbers: 42002238 and 41872057).

Appendix A. Supplementary data

Supplementary data to this article can be found online at https://doi.org/10.1016/j.precamres.2020.106078.

References

Altherr, R., Holl, A., Hegner, E., Langer, C., Kreuzer, H., 2000. High-K calc-alkaline I-type plutonism in the European Variscides, northern Vosges (France) and northern Schwarzwald (Germany). Lithos 50, 51–73.
Anhaeusser, C.R., 2014. Archaean greenstone belts and associated rocks–a review. J. Africa Earth Sci. 100, 684–732.
Arndt, N.T., 2013. The formation and evolution of the continental crust. Geochem. Perspect. 2, 405–533.
Arth, J.G., Barker, F., 1976. Rare-earth partitioning between hornblende and dacitic liquid and implications for the genesis of trondhjemitic–tonalitic magmas. Geology 4, 534–536.
Atherton, M.P., Petford, N., 1993. Generation of sodium-rich magmas from newly underplated basaltic crust. Nature 362, 144–146.
Bai, X., Liu, S.W., Yan, M., Zhang, L.F., Wang, W., Guo, R.R., Guo, B.R., 2014. Geological event series of Early Precambrian metamorphic complex in South Fushun area, Liaoning Province. Acta Petrol. Sinica 30, 2905–2924 (in Chinese with English abstract).
Bédard, J.H., 2006. A catalytic delamination-driven model for coupled genesis of Archaean crust and sub-continental lithospheric mantle. Geochim. Cosmochim. Acta 70, 1188–1214.
Beard, J., Lofgren, G.E., 1991. Dehydration melting and water-saturated melting of basaltic and andesitic greenstones and amphibolites at 1, 3 and 6.9 kbar. J. Petrol. 32, 465–501.
Belousova, E.A., Griffin, W.L., O'Reilly, S.Y., Fisher, N.I., 2002. Igneous Zircon: Trace element composition as an indicator of source rock type. Contrib. Miner. Petrol. 143, 602–622.
Bodinier, J.L., Godard, M., 2014. Orogenic, ophiolitic and abyssal peridotites. Treat. Geochem. 2, 103–167.
Boniface, N., Schenk, V., Appel, P., 2012. Paleoproterozoic eclogites of MORB-type chemistry and three Proterozoic orogenic cycles in the Ubendian Belt (Tanzania): evidence from monazite and zircon geochronology, and geochemistry. Precambr. Res. 192, 16–33.
Castillo, P.R., 2012. Adakite petrogenesis. Lithos 134–135, 304–316.
Castillo, P.R., Janney, P.E., Solidum, R., 1999. Petrology and geochemistry of Camiguin Island, southern Philippines: insights into the source of adakite and other lavas in a complex arc tectonic setting. Contrib. Miner. Petrol. 134, 33–51.
Chappell, B.W., White, A.J.R., 1992. I- and S-type granites in the Lachlan Fold Belt. Transactions of the Royal Society of Edinburgh. Earth Sci. 83, 1–26.
Chen, B., Chen, Z.C., Jahn, B.M., 2009. Origin of mafic enclaves from the Taihang Mesozoic orogen, north China craton. Lithos 110, 343–358.
Clark, C., Collins, A.S., Timms, N.E., Kinny, P.D., Chetty, T.R.K., Santosh, M., 2009. SHRIMP U-Pb age constraints on magmatism and high-grade metamorphism in the Salem Block, southern India. Gondwana Res. 16, 27–36.
Clark, C., Kinny, P.D., Harley, S.L., 2012. Sedimentary provenance and age of metamorphism of the Vestfold Hills, East Antarctica: evidence for a piece of Chinese Antarctica? Precambr. Res. 196–197, 23–45.
Condie, K.C., 1981. Archean Greenstone Belts. Elsevier, Amsterdam, p. 434.
Condie, K.C., 1986. Origin and early growth rate of continents. Precambr. Res. 32, 261–278.
Condie, K.C., 1994. Greenstones through time. In: Condie, K.C. (Ed.), Archean Crustal Evolution. Elsevier, Amsterdam, pp. 85–120.
Condie, K.C., 1998. Episodic continental growth and supercontinents: a mantle avalanche connection? Earth Planet. Sci. Lett. 163, 97–108.
Condie, K.C., 2005. High field strength element ratios in Archean basalts: a window to evolving sources of mantle plumes? Lithos 79, 491–504.
Condie, K.C., Kröner, A., 2011. The building blocks of continental crust: evidence for a major change in the tectonic setting of continental growth at the end of the Archean. Gondwana Res. 23, 394–402.
Corfu, F., Hanchar, J.M., Hoskin, P.W.O., Kinny, P., 2003. Atlas of Zircon Textures. Rev. Mineral. Geochem. 53, 469–500.
Defant, M.J., Drummond, M.S., 1990. Derivation of some modern arc magmas by melting of young subducted lithosphere. Nature 347, 662–665.
Dubińska, E., Bylina, P., Kozłowski, A., Dörrc, W., Nejbert, K., Schastok, J., Kulicki, C., 2004. U-Pb dating of serpentinization: hydrothermal zircon from a metasomatic rodingite shell (Sudetic ophiolite, SW Poland). Chem. Geol. 203, 183–203.
Eiler, J.M., Grawford, A.J., Elliott, T.R., Farley, K.A., Valley, J.W., Stolper, E., 2000. Oxygen isotope geochemistry of oceanic arc lavas. J. Petrol. 41, 229–256.
Foley, S.F., Tiepolo, M., Vannucci, R., 2002. Growth of early continental crust controlled by melting of amphibolite in subduction zones. Nature 417, 637–640.
Geng, Y.S., Liu, F.L., Yang, C.H., 2006. Magmatic event at the end of the Archean in Eastern Hebei Province and its geological implication. Acta Geol. Sinica 80, 819–833.
Geng, Y.S., Du, D.L., Ren, L.D., 2012. Growth and reworking of the early Precambrian continental crust in the North China Craton: constraints from zircon Hf isotopes. Gondwana Res. 21, 517–529.
Grant, M.L., Wilde, S.A., Wu, F., Yang, J., 2009. The application of zircon cathodoluminescence imaging, Th–U–Pb chemistry and U-Pb ages in interpreting

discrete magmatic and high-grade metamorphic events in the North China Craton at the Archean/Proterozoic boundary. Chem. Geol. 261, 155–171.
Gill, J.B., 1981. Orogenic Andesites and Plate Tectonics. Springer Verlag, New York, pp. 1–385.
Griffin, W.L., Doyle, B.J., Ryan, C.G., Pearson, N.J., O'Reilly Suzanne, Y., Davies, R., Kivi, K., Van Achterbergh, E., Natapov, L.M., 1999. Layered mantle lithosphere in the Lac de Gras Area, Slave Craton: composition, structure and origin. J. Petrol. 40, 705–727.
Griffin, W.L., Pearson, N.J., Belousova, E.A., O'Reilly, S.Y., van Achterberg, E., Shee, S. R., 2000. The Hf-isotope composition of cratonic mantle: LAM-MC-ICPMS analysis of zircon megacrysts in kimberlites. Geochim. Cosmochim. Acta 64, 133–147.
Grove, T.L., Donnelly-Nolan, M., 1986. The evolution of young sillic lavas at Medicine Lake Volcano, California: implications for the origin of compositional gaps in calc-alkaline series lavas. Contrib. Miner. Petrol. 92, 281–302.
Grove, T.L., Elkins Tanton, L.T., Parman, S.W., Cartterjee, N., Muntener, O., Gaetani, G. A., 2003. Fractional crystallization and mantle melting controls on calk-alkaline differentiation trends. Contrib. Miner. Petrol. 145, 515–533.
Irvine, T.H., Baragar, W.R.A., 1971. A guide to the chemical classification of the common volcanic rocks. Can. J. Earth Sci. 8, 523–548.
Jiang, N., Guo, J., Zhai, M., Zhang, S., 2010. ~2.7 Ga crust growth in the North China craton. Precambr. Res. 179, 37–49.
Hawkesworth, C., Kemp, A., 2006. Evolution of the continental crust. Nature 443, 811–817.
Hill, R.I., Chappell, B.W., Campbell, I.H., 1992. Late Archaean granites of the southeastern Yilgarn Block, Western Australia: age, geochemistry, and origin. Trans. R. Soc. Edinburgh: Earth Sci. 83, 211–226.
Hollings, P., Wyman, D.A., Kerrich, R., 1999. Komatiite–basalt–rhyolite volcanic associations in northern Superior Province greenstone belts: significance of plume–arc interaction in the generation of the proto-continental Superior Province. Lithos 46, 137–161.
Kay, R.W., 1978. Aleutian magnesian andesites: melts from subducted Pacific Ocean crust. J. Volcanol. Geoth. Res. 4, 117–132.
Kelemen, P.B., 1995. Genesis of high $Mg^{\#}$ andesites and the continental crust. Contrib. Miner. Petrol. 120, 1–19.
Klein, M., Stosch, H.G., Seck, H.A., 1997. Partitioning of high field-strength and rare-earth elements between amphibole and quartz-dioritic to tonalitic melts: an experimental study. Chem. Geol. 138, 257–271.
Lackey, J.S., 2005. The Magmatic and Alteration History of the Sierra Nevada Batholith as Recorded by Oxygen Isotope Ratios in Zircon, Titanite, Garnet, and Quartz. PhD Thesis. University of Wisconsin.
Lee, C.T., Yin, Q., Rudnick, R.L., Jacobsen, S.B., 2001. Preservation of ancient and fertile lithospheric mantle beneath the southwestern United States. Nature 411, 69.
Li, J.J., Shen, B.F., 2000. Geochronology of Precambrian continental crust in Liaoning Province and Jilin Province. Prog. Precambrian Res. 23, 249–255 (in Chinese with English abstract).
Li, Z., Wei, C.J., 2017. Two types of Neoarchean basalts from Qingyuan greenstone belt, North China Craton: petrogenesis and tectonic implications. Precambr. Res. 292, 175–193.
Li, Z., Chen, B., 2019. Lithotectonic elements of Archean basement on the Liaodong Peninsula and its vicinity, North China Craton. Front. Earth Sci. 13, 209–228.
Li, Z., Chen, B., Wei, C.J., 2017. Is the Paleoproterozoic Jiao–Liao–Ji Belt (North China Craton) a rift? Int. J. Earth Sci. 106, 355–375.
Li, Z., Chen, B., Wang, J.L., 2016a. Geochronological framework and geodynamic implications of mafic magmatism in the Liaodong Peninsula and adjacent regions, North China Craton. Acta Geol. Sinica (English Edition) 90, 138–153.
Li, Z., Chen, B., Wei, C.J., 2016b. Hadean detrital zircon in the North China Craton. J. Mineral. Petrol. Sci. 111, 283–291.
Li, Z., Chen, B., Yan, X.L., 2019a. The Liaohe Group: an insight into the Paleoproterozoic tectonic evolution of Jiao-Liao-Ji Belt, North China Craton. Precambr. Res. 326, 174–195.
Li, Z., Wei, C.J., Zhang, S.W., Yang, C., Duan, Z.Z., 2019b. Neoarchean granitoid gneisses in Eastern Hebei, North China Craton: revisited. Precambr. Res. 324, 62–85.
Li, Z., Meng, E., Wang, C.Y., Li, Y.G., 2019c. Early Precambrian tectonothermal events in the Southern Jilin Province, China: Implications for Neoarchean crustal evolution of the northeastern North China Craton. Mineral. Petrol. 113, 185–205.
Li, Z., Wei, C.J., Chen, B., Fu, B., Gong, M.Y., 2020. Late Neoarchean reworking of the Mesoarchean crustal remnant in northern Liaoning, North China Craton: a U-Pb–Hf–O–Nd perspective. Gondwana Res. 80, 350–369.
Liu, H., Zhang, H.F., 2019. Paleoproterozoic ophiolite remnants in the northern margin of the North China Craton: evidence from the Chicheng peridotite massif. Lithos 344–345, 311–323.
Liu, D.Y., Wilde, S.A., Wan, Y.S., Wu, J.S., Zhou, H.Y., Dong, C.Y., Yin, X.Y., 2008. New U-Pb and Hf isotopic data confirm Anshan as the oldest preserved segment of the North China Craton. Am. J. Sci. 308, 200–231.
Liu, J., Liu, Z.H., Zhao, C., Wang, C.J., Peng, Y.B., Zhang, H., 2017. Petrogenesis and zircon LA-ICP-MS U-Pb dating of newly discovered Mesoarchean gneisses on the northern margin of the North China Craton. Int. Geol. Rev. 59, 1575–1589.
Lodge, R.W.D., 2016. Petrogenesis of intermediate volcanic assemblages from the Shebandowan greenstone belt, Superior Province: evidence for subduction during the Neoarchean. Precambr. Res. 272, 150–167.
Mahoney, J.J., Storey, M., Duncan, R.A., Spencer, K.J., Pringle, M.S., 1993. Geochemistry and age of the Ontong Java Plateau. In: Pringle, M.S., Sager, W.W., Sliter, W.V., Stein, S. (Eds.), The Mesozoic Pacific: Geology, Tectonics and Volcanism. AGU, Washington D.C., pp. 233–261
Maibam, B., Gerdes, A., Goswami, J.N., 2016. U-Pb and Hf isotope records in detrital and magmatic zircon from eastern and western Dharwar craton, southern India: evidence for coeval Archaean crustal evolution. Precambr. Res. 275, 496–512.
Martin, H., 1986. Effect of steeper Archean geothermal gradient on geochemistry of subduction-zone magmas. Geology 14, 753–756.
Martin, H., 1994. The Archean grey gneisses and the genesis of the continental crust. In: Crustal, A., Condie, K.C. (Eds.), Evolution. Developments in Precambrian Geology. Elsevier, Amsterdam, pp. 205–259.
Martin, H., 1999. Adakitic magmas: modern analogues of Archaean granitoids. Lithos 46, 411–429.
Martin, H., Smithies, R.H., Rapp, R., Moyen, J.F., Champion, D., 2005. An overview of adakite, tonalite–trondhjemite–granodiorite (TTG), and sanukitoid: relationships and some implications for crustal evolution. Lithos 79, 1–24.
Middlemost, E.A., 1994. Naming materials in the magma/igneous rock system. Earth Sci. Rev. 37, 215–224.
Moyen, J.F., 2009. High Sr/Y and La/Yb ratios: the meaning of the "adakitic signature". Lithos 112, 556–574.
Moyen, J.F., 2011. The composite Archaean grey gneisses: petrological significance, and evidence for a non-unique tectonic setting for Archaean crustal growth. Lithos 123, 21–36.
Moyen, J.F., Stevens, G., 2006. Experimental constraints on TTG petrogenesis: Implications for Archean geodynamics. In: Benn, K., Mareschal, J.C., Condie, K.C. (Eds.), Archean Geodynamics and Environments. American Geophysical Union, Washington, pp. 149–178.
Noyes, H., Frey, F.A., Wones, D.R., 1983. A tale of two plutons: geochemical evidence bearing on the origin and differentiation of the Red Lake and Eagle Peak plutons, central Sierra Nevada, California. J. Geol. 91, 487–509.
Ordóñez-Calderón, J.C., Polat, A., Fryer, B.J., Appel, P.W.U., van Gool, J.A.M., Dilek, Y., Gagnon, J.E., 2009. Geochemistry and geodynamic origin of the Mesoarchean Ujarassuit and Ivisaartoq greenstone belts, SW Greenland. Lithos 113, 133–157.
Polat, A., Kusky, T., Li, J.H., Fryer, B., Kerrich, R., Patrick, K., 2005. Geochemistry of Neoarchean (ca. 2.55–2.50 Ga) volcanic and ophiolitic rocks in the Wutaishan greenstone belt, central orogenic belt, North China craton: implications for geodynamic setting and continental growth. Geol. Soc. Am. Bull. 117, 1387–1399.
Peng, P., Wang, C., Wang, X.P., Yang, S.Y., 2015. Qingyuan high-grade granite–greenstone terrain in the Eastern North China Craton: root of a Neoarchaean arc. Tectonophysics 662, 7–21.
Rapp, R.P., Watson, E.B., 1995. Dehydration melting of metabasalt at 8–32 kbar: implications for continental growth and crust-mantle recycling. J. Petrol. 36, 891–931.
Rapp, B.R., Shimizu, N., Norman, M.D., Applegate, G.S., 1999. Reaction between slab derived melts and peridotite in the mantle wedge: experimental constraints at 3.8 GPa. Chem. Geol. 160, 335–356.
Révillon, S., Hallot, E., Arndt, N.T., Chauvel, C., Duncan, R.A., 2000. A complex history for the Caribbean Plateau: petrology, geochemistry and geochronology of the Béata Ridge, South Hispaniola. J. Geol. 108, 641–661.
Rollision, H.R., 1993. Using Geochemical Data: Evaluation, Presentation, Interpretation. Longma Singapore Publishers (Pte) Ltd, Singapore.
Ronov, A.B., Yaroshevsky, A.A., 1976. A new model for the chemical structure of the Earth's crust. Geokhimiya 13, 89–121.
Shen, B.F., Li, J.J., Mao, D.B., 1997. Geological features types and evolution of greenstone belts in the North China Platform. Progr. Precambrian Res. 20, 2–11 (in Chinese with English abstract).
Sklyarov, E.V., Fedorovsky, V.S., 2006. Magma mingling: tectonic and geodynamic aspects. Geotektonika 2, 47–64.
Smithies, R.H., 2000. The Archaean tonalite–trondhjemite–granodiorite (TTG) series is not an analogue of Cenozoic adakite. Earth Planet. Sci. Lett. 182, 115–125.
Smithies, R.H., Champion, D.C., Cassidy, K.F., 2003. Formation of Earth's early Archaean continental crust. Precambr. Res. 127, 89–101.
Song, B., Nutman, A.P., Liu, D.Y., Wu, J.S., 1996. 3800–2500 Ma crust in the Anshan area of Liaoning Province, northeastern China. Precambr. Res. 78, 79–94.
Stern, C.R., Kilian, R., 1996. Role of subducted slab, mantle wedge and continental crust in the generation of adakites from the Andean Austral Volcanic Zone. Contrib. Miner. Petrol. 123, 263–281.
Sun, S.S., McDonough, W.F., 1989. Chemical and isotopic systematics of oceanic basalts: implications for mantle composition and processes. Geol. Soc. Spec. Pubicat., London 42, 313–345.
Tang, M., Wang, X.L., Shu, X.J., Wang, D., Yang, T., Gopon, P., 2014. Hafnium isotopic heterogeneity in zircons from granitic rocks: geochemical evaluation and modeling of zircon effect in crustal anatexis. Earth Planet. Sci. Lett. 389, 188–199.
Tomaschek, F., 2003. Zircons from Syros, Cyclades, Greece–recrystallization and mobilization of zircon during high pressure metamorphism. J. Petrol. 44, 1977–2002.
Valley, J.W., Chiarenzelli, J.R., McLelland, J.M., 1994. Oxygen isotope geochemistry of zircon. Earth Planet. Sci. Lett. 126, 187–206.
Valley, J.W., Bindeman, I.N., Peck, W.H., 2003. Empirical calibration of oxygen isotope fractionation in zircon. Geochim. Cosmochim. Acta 67, 3257–3266.
Valley, J.W., Lackey, J.S., Cavosie, A.J., Clechenko, C.C., Spicuzza, M.J., Basei, M.A.S., Bindeman, I.N., Ferreira, V.P., Sial, A.N., King, E.M., Peck, W.H., Sinha, A.K., Wei, C. S., 2005. 4.4 billion years of crustal maturation: oxygen isotope ratios of magmatic zircon. Contrib. Mineral. Petrol. 150, 561–580.
Wan, Y.S., Song, B., Yang, C., Liu, D.Y., 2005a. Zircon SHRIMP U-Pb geochronology of Archaean rocks from the Fushun-Qingyuan Area, Liaoning Province and its geological significance. Acta Geol. Sin. 79, 78–87 (in Chinese with English abstract).

Wan, Y.S., Song, B., Yang, C., Liu, D.Y., 2005b. Geochemical characteristics of Archaean basement in the Fushun-Qingyuan area, northern Liaoning Province and its geological significance. Geol. Rev. 51, 128–137 (in Chinese with English abstract).
Wan, Y.S., Liu, D.Y., Song, B., Wu, J.S., Yang, C.H., Zhang, Z.Q., Geng, Y.S., 2005c. Geochemical and Nd isotopic compositions of 3.8 Ga meta-quartz dioritic and trondhjemitic rocks from the Anshan area and their geological significance. J. Asian Earth Sci. 24, 563–575.
Wan, Y.S., Liu, D.Y., Nutman, A.P., Zhou, H.Y., Dong, C.Y., Yin, X.Y., Ma, M.Z., 2012. Multiple 3.8–3.1 Ga tectono-magmatic events in a newly discovered area of ancient rocks (the Shengousi Complex), Anshan, North China Craton. J. Asian Earth Sci. 54–55, 18–30.
Wang, W., Liu, S.W., Cawood, P.A., Bai, X., Guo, R.R., Guo, B.R., Wang, K., 2016a. Late Neoarchean subduction-related crustal growth in the Northern Liaoning region of the North China Craton: Evidence from ~2.55 to 2.50 Ga granitoid gneisses. Precambr. Res. 281, 200–223.
Wang, M.J., Liu, S.W., Wang, W., Wang, K., Yan, M., Guo, B.R., Bai, X., Guo, R.R., 2016b. Petrogenesis and tectonic implications of the Neoarchean North Liaoning tonalitic-trondhjemitic gneisses of the North China Craton, North China. J. Asian Earth Sci. 131, 12–39.
Wang, C., Song, S.G., Wei, C.J., Su, L., Allen, M.B., Niu, Y.L., Li, X.H., Dong, J.L., 2019. Palaeoarchaean deep mantle heterogeneity recorded by enriched plume remnants. Nat. Geosci. 12, 672–678.
Wang, D., Romer, R.L., Guo, J.H., Glodny, J., 2020. Li and B isotopic fingerprint of Archean subduction. Geochim. Cosmochim. Acta 268, 446–466.
Whattam, S.A., Stern, R.J., 2011. The 'subduction initiation rule': a key for linking ophiolites, intra-oceanic forearcs, and subduction initiation. Contrib. Miner. Petrol. 162, 1031–1045.
White, A.J.R., Chappell, B.W., Wyborn, D., 1999. Application of the restite model to the Deddick granodiorite and its enclaves — a reinterpretation of the observations and data of Maas et al. (1997). J. Petrol., 40, 413–421.
Wilson, W., 1989. Igneous Petrogenesis. Unwin Hyman, London, pp. 327–373.
Windley, B.F., 1995. The Evolving Continents. John Wiley and Sons, New York, pp. 1–544.
Wu, F.Y., Li, X.H., Yang, J.H., Zheng, Y.F., 2007. Discussion on the petrogenesis of granites. Acta Petrol. Sinica 23, 1217–1238 (in Chinese with English Abstract).
Wu, K.K., Zhao, G.C., Sun, M., Yin, C.Q., He, Y.H., Tam, P.Y., 2013. Metamorphism of the northern Liaoning Complex: implications for the tectonic evolution of Neoarchaean basement of the Eastern Block, North China Craton. Geosci. Front. 4, 305–320.
Wu, M.L., Lin, S.F., Wan, Y.S., Gao, J.F., 2016. Crustal evolution of the Eastern Block in the North China Craton: Constraints from zircon U-Pb geochronology and Lu–Hf isotopes of the Northern Liaoning Complex. Precambr. Res. 275, 35–47.
Xie, Q., Kerrich, R., Fan, J., 1993. HFSE/REE fractionations recorded in the three komatiite-basalt sequences, Archean Abitibi belt: implications for multiple plume sources and depth. Geochim. Cosmochim. Acta 57, 4111–4118.
Xiong, X.L., Adam, J., Green, T.H., 2005. Rutile stability and rutile/melt HFSE partitioning during partial melting of hydrous basalt: Implications for TTG genesis. Chem. Geol. 218, 339–359.
Yang, C., Wei, C.J., 2017a. Ultrahigh temperature (UHT) mafic granulites in the East Hebei, North China Craton: Constraints from a comparison between temperatures derived from REE-based thermometers and major element-based thermometers. Gondwana Res. 46, 156–169.
Yang, C., Wei, C.J., 2017b. Two phases of granulite facies metamorphism during the Neoarchean and Paleoproterozoic in the East Hebei, North China Craton: records from mafic granulites. Precambr. Res. 301, 49–64.
Yang, J.H., Wu, F.Y., Wilde, S.A., Zhao, G.C., 2008. Petrogenesis and geodynamics of Late Archean magmatism in eastern Hebei, eastern North China Craton: geochronological, geochemical and Nd–Hf isotopic evidence. Precambr. Res. 167, 125–149.
Zhai, M.G., Santosh, M., 2013. Metallogeny of the North China Craton: link with secular changes in the evolving Earth. Gondwana Res. 24, 275–297.
Zhai, M.G., Yang, R.Y., Lu, W.J., Zhou, J.E., 1985. Geochemistry and evolution of the Qingyuan Archaean granite–greenstone terrain, NE China. Precambr. Res. 27, 37–62.
Zhang, H.F., Ying, J.F., Santosh, M., Zhao, G.C., 2012a. Episodic growth of Precambrian lower crust beneath the North China Craton. A synthesis. Precambrian Res. 222–223, 255–264.
Zhang, H.F., Yang, Y.H., Santosh, M., Zhao, X.M., Ying, J.F., Xiao, Y., 2012b. Evolution of the Archean and Paleoproterozoic lower crust beneath the Trans-North China Orogen and the Western Block of the North China Craton. Gondwana Res. 22, 73–85.
Zhang, H.F., Wang, J.L., Zhou, D.W., Yang, Y.H., Zhang, G.W., Santosh, M., Yu, H., Zhang, J., 2014. Hadean to Neoarchean episodic crustal growth: detrital zircon records in Paleoproterozoic quartzites from the southern North China Craton. Precambr. Res. 254, 245–257.
Zhao, G.C., Zhai, M.G., 2013. Lithotectonic elements of Precambrian basement in the North China Craton: review and tectonic implications. Gondwana Res. 23, 1207–1240.
Zhao, G.C., Wilde, S.A., Cawood, P.A., Lu, L.Z., 1998. Thermal evolution of Archean basement rocks from the eastern part of the North China Craton and its bearing on tectonic setting. Int. Geol. Rev. 40, 706–721.
Zhao, G.C., Wilde, S.A., Cawood, P.A., Sun, M., Lu, L.Z., 2001. Archaean blocks and their boundaries in the North China Craton: lithological, geochemical, structural and P-T path constraints. Precambr. Res. 107, 45–73.
Zhao, G.C., Sun, M., Wilde, S.A., Li, S.Z., 2005. Late Archean to Paleoproterozoic evolution of the North China Craton: key issues revisited. Precambr. Res. 136, 177–202.
Zhao, G.C., Cawood, P.A., Li, S.Z., Wilde, S.A., Sun, M., Zhang, J., He, Y.H., Yin, C.Q., 2012. Amalgamation of the North China Craton: key issues and discussion. Precambr. Res. 222–223, 55–76.